Control of Vortex Shedding from a Circular Cylinder using Imposed Transverse Magnetic Field

Sintu Singha and K. P. Sinhamahapatra
Department of Aerospace Engineering, IIT Kharagpur
Kharagpur 721302, India

Abstract

The flow of a conducting fluid past a circular cylinder placed centrally in a channel subjected to an imposed transverse magnetic field has been simulated to study the effect of a magnetic field on vortex shedding at different Reynolds numbers varying from 50 to 250. The two-dimensional incompressible laminar viscous flow equations are solved using a second-order implicit unstructured collocated grid finite volume method. An imposed transverse magnetic field markedly reduces the unsteady lift amplitude indicating a reduction in the strength of the shed vortices. It is observed, that the periodic vortex shedding at the higher Reynolds numbers can be completely suppressed if a sufficiently strong magnetic field is imposed. The required magnetic field strength to suppress shedding increases with Reynolds number. The simulation shows that the separated zone behind the cylinder in a steady flow is reduced as the magnetic field strength is increased. Due attention is given to resolve and study the unsteady cylinder wake and its interaction with the shear-layer on the channel wall in the presence of a magnetic field. A critical value of the Hartmann number for complete suppression of the shedding at a given Reynolds number is found.

Keywords: transverse magnetic field, Hartmann number, vortex shedding, wake, circular cylinder, separation

Introduction

The flow over a circular cylindrical body is a common phenomenon in many engineering applications. The flow is essentially unsteady except at very low Reynolds numbers less than about 50. The steady flow at a low Reynolds number is characterized by steady separation and a closed near wake of recirculating flow. At relatively higher Reynolds numbers, the relevant unsteady flows are characterized by the periodic shedding of vortices and unsteady separated vortex wake. The unsteady flow exerts fluctuating forces on the immersed bodies. The fluctuating forces on the bluff body may cause the body to vibrate, which may be severe for a range of natural frequency to the vortex shedding frequency ratio, particularly if the mass ratio and damping are low. The control of such 'flow-induced vibration' can be achieved if the vortex shedding and/or the size of the separated zone behind the body are controlled. An imposed transverse magnetic field does the job satisfactorily when the fluid is electrically conducting. The use of magnetic field in the cross-stream direction is a novel method of controlling the separated zone behind the body, which in turn helps to reduce or eliminate the periodic vortex shedding and the resulting flow-induced vibration in a conducting fluid. Bramley [1974a, 1974b] studied the steady two-dimensional incompressible MHD flow past a circular cylinder with an applied magnetic field parallel to the main flow using analytical and numerical methods. It was observed that with an applied magnetic field the flow remained attached to the cylinder longer and in some cases did not separate until the

rear stagnation point. Gerbeth et al. [1990] studied steady unidirectional MHD flow around a cylinder driven by crossed electric and magnetic fields analytically using series solution. Josserand et al. [1993] studied the effect of an aligned magnetic field in the flow of a liquid metal past a cylinder and observed that the magnetic field could reduce the drag on the cylinder and the Karman street behind the cylinder was suppressed for a sufficient value of the magnetic field. Mutschke et al. [1998] studied the controlling influence of external magnetic field on the wake instabilities in the flow of an electrically conducting fluid around a circular cylinder. Midya et al. [2003] investigated the magnetohydrodynamic effect on viscous flow in a channel with constriction. It was observed that the transverse magnetic field reduced the size of the separated zone downstream of the constriction and the separation could be eliminated with a large magnetic field. The wall shear stress, however, increased with the strength of the imposed magnetic field. Sekhar et al. [2006] investigated laminar flow past a circular cylinder subjected to inline magnetic field and observed that parallel magnetic field reduced the wake length. Singha et al. [2007] studied the effect of an applied transverse magnetic field on steady as well as periodic vortex-shedding flow around a square cylinder using an explicit staggered grid finite difference method. Recently Knaepen et al. [2004], Kassinos et al. [2007], Sarris et al. [2007] have studied the structure of MHD turbulence and transport processes in MHD turbulent flows under different conditions using LES and DNS techniques.

In the present work, the incompressible viscous flow of an electrically conducting fluid around a circular cylinder confined symmetrically between two parallel walls in the presence of a uniform transverse magnetic field is studied numerically. The incompressible Navier-Stokes equations are solved using an unstructured collocated grid finite volume method. The solution is advanced in time using a second-order implicit scheme. The study is performed at several Reynolds numbers over a range of magnetic-field strength expressed in terms of the nondimensional Hartmann number. The study shows that the separated wake length decreases with the increase in magnetic field for steady flow cases. The imposed magnetic field reduces the strength of the shed vortices and, hence, reduces the flow asymmetry and lift amplitude in unsteady flows at higher Reynolds numbers. Moreover, the unsteady flows at higher Reynolds numbers can be made steady when the applied magnetic field is sufficiently strong.

Configuration and Numerical Method

The configuration considered is a two dimensional incompressible viscous flow of electrically conducting fluid with constant conductivity σ and density ρ around a circular cylinder of diameter D placed symmetrically between two flat plates as in Figure 1. A uniform magnetic field (B_0) is imposed along the cross-flow direction. The distance between the two plane walls (H) is 4D. A parabolic streamwise velocity $u_1 = V\left[1-4\left(\frac{y}{H}\right)^2\right]$ is specified at the inlet, where V is the centerline velocity. A plane solid wall near a circular cylinder can suppress the vortex shedding from the cylinder if the gap between them is less than a critical value corresponding to the Reynolds number (Zovatto and Pedrizetti, 2001). However, a gap space of 1.5D corresponding to the channel height of 4D is well above the critical height for suppression of the shedding due to wall influence for $\mathrm{Re} \geq 100$.

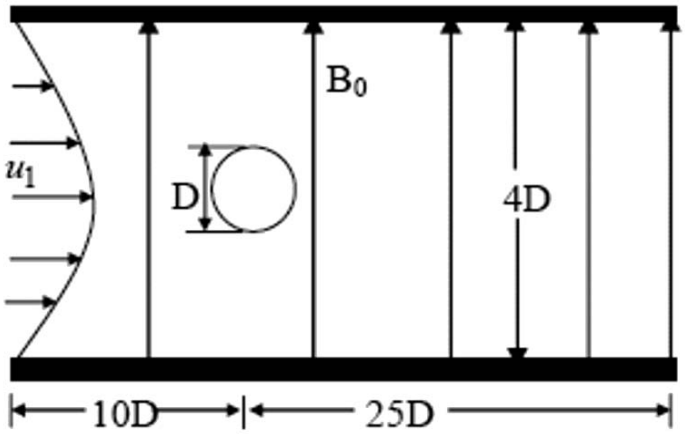

Figure 1. The computational flow domain

Due to magnetohydrodynamic interactions, an induced electric field E_z is produced in the direction perpendicular to the plane of the flow, which in turn produces an induced magnetic field in the streamwise direction. It is assumed that the flows considered are of very small magnetic Reynolds number $\mathrm{Re}_m (= \mu\sigma VD$, where V is the characteristic velocity and μ is the permeability) and, hence, the induced magnetic field is negligible so that there is no distortion in the imposed magnetic field (Shercliff, 1965). It is also assumed that the magnetic field is not distorted near the body due to the differences in permeability and conductivity between the solid body and the conducting fluid. Thus, a short-circuited situation is assumed as if the induced current is taken through a stationary closed loop made of perfect conductor lying in the direction perpendicular to the stream. Consequently, the induced electric field (E_z) becomes zero (Shercliff, 1965) and a net current $\sigma B_0 Q$ flows normal to the plane of the flow, where Q is the fluid volume flow rate. It is further assumed that the electric field due to the polarization of charges is negligible. An elegant justification for these assumptions is given by Midya et al. [2003] for the flow of a conducting fluid in a channel with constriction. The presence of a body in the flow, which usually will have a different conductivity, may reduce the accuracy of some of the assumptions. The induced magnetic and electric fields will alter the current flow and the current continuity needs to be taken in to account for better accuracy. However, when the conductivities of the flowing fluid and the cylinder material are nearly of the same order of magnitude and the Hartmann number is small, the induced electric and magnetic fields will not be large enough to have significant effect on the overall flow behavior. With this assumption, the current continuity is not considered in the present study and it is felt that the solution will be able to capture the dominant features of the flow both qualitatively and quantitatively. With the consideration of the Lorentz forces due to the external magnetic field and the assumptions stated above, the governing equations for two-dimensional flows in their nondimensional form are given by

$$\frac{\partial u_i}{\partial x_i} = 0 \tag{1}$$

$$\frac{\partial u_i}{\partial t} + \frac{\partial}{\partial x_j}(u_j u_i) = -\frac{\partial p}{\partial x_i} + \frac{1}{\mathrm{Re}}\frac{\partial^2 u_i}{\partial x_j \partial x_j} - \frac{H_m^2}{\mathrm{Re}} K_i u_i \tag{2}$$

In equation (2), $K_1 = 1$, $K_2 = 1$ and Re is the Reynolds number VD/υ with υ being the kinematic viscosity. The characteristic velocity V is taken as the centerline inflow velocity and the Hartmann number (H_m) is defined as $H_m = B_0 D\sqrt{\sigma/\rho\upsilon}$.

The governing equations (1) and (2) are numerically solved using an unstructured cell-centered collocated grid finite volume method. Integrated over a small control volume, which in this case is a triangular cell of the mesh, the equations can be written as

$$\oint_S \mathbf{V}\cdot\hat{\mathbf{n}}dS = 0 \tag{3}$$

$$\frac{\partial}{\partial t}\int_\Omega u_i d\Omega + \oint_S u_i \mathbf{V}\cdot\hat{\mathbf{n}}dS = -\oint_S p n_i dS + \frac{1}{\mathrm{Re}}\oint_S \nabla u_i \cdot\hat{\mathbf{n}}dS - \frac{H_m^2}{\mathrm{Re}}\int_\Omega K_i u_i d\Omega \tag{4}$$

where $\mathbf{V}$ is the velocity vector of the fluid element, Ω and S denote the nondimensional control volume and the bounding surface of the control volume respectively. The unit vector normal to the surface S is $\hat{\mathbf{n}}$ and n_i denotes the Cartesian component of the unit normal vector.

The convective terms in the momentum equation for a cell are computed as the sum of fluxes across the three faces where the flux across each face is computed as a product of the outward mass flux and the appropriate cell face velocity component. The velocity on a face is obtained using a quadratic upwind interpolation (Leonard, 1979) from the velocity at three points. Two of these three points are the cell centers on either side of the face and the third point is the projection of the distant vertex of the upstream triangle on the line joining the two cell centers.

The diffusive terms in the momentum equation integrated over a triangular control volume is expressed in the following generic form:

$$F_{ij}^{v} = \int_\Omega \frac{\partial}{\partial x_i}\left(\frac{\partial\phi}{\partial x_j}\right)d\Omega \qquad i, j = 1, 2;$$

$$= \oint_S \left(\frac{\partial\phi}{\partial x_j}\right)n_i dS \qquad \approx \sum_{k=1}^{3}\frac{\partial\phi}{\partial x_{jk}}n_{ik}dS_k\,, \tag{5}$$

The gradients along the face of a control volume are computed using the values of the variable at the two adjacent cell centers and at the two terminating vertices of the face. The value of the variable ϕ at a vertex of the face is obtained by an interpolation from the cell-centered values of the surrounding cells using the linearity-preserving Laplacian due to Holmes and Connel [1989]. The procedure provides the diffusive flux terms for a cell with center P in terms of the variable at P and at the center of all the neighboring cells shared by the vertices of the cell P.

$$F_{ij}^{\nu} = a_P\phi_P + \sum_{m\neq P}^{N_1} c_m\phi_m + \sum_{m\neq P}^{N_2} d_m\phi_m + \sum_{m\neq P}^{N_3} e_m\phi_m \tag{6}$$

where N_1, N_2, N_3 are the number of cells connected to the three vertices of the triangular cell P.

The source term in the momentum equation representing the Lorentz force is discretized using the cell-centered variables and the cell volume. The solution is advanced in time using the implicit Crank-Nicolson scheme. The discretized equation is written in the form

$$\frac{u_{iP}^{n+1}-u_{iP}^{n}}{\Delta t} + \frac{1}{2}\left(\sum_f m_f^{n+1}u_{if}^{n+1} + \sum_f m_f^{n}u_{if}^{n}\right) = -\sum_f p_f^{n+1}n_{if}dS_f + \frac{1}{2}\left(\sum_f F_{dif}^{n+1} + \sum_f F_{dif}^{n}\right) + \frac{1}{2}\left(L_{iP}^{n+1} + L_{iP}^{n}\right) \tag{7}$$

where P and f denote the cell-centre and a cell face respectively. F_d is the diffusive flux term, L is the Lorentz force source term and m is mass flux. The index i =1, 2 denotes the streamwise (x) and cross-stream (y) direction respectively. The above equation is solved along with the discretized continuity equation written as

$$\sum_f m_f^{n+1} = 0 \tag{8}$$

A provisional velocity field $\left(\mathbf{V}^*\right)$ is first computed using the latest available mass flux and dropping the pressure term from the equation (7). The modified equation is solved using a Gauss-Seidel iterative solver. The provisional velocity field is used to compute the cell face velocities using the Rhie and Chow [1983] interpolation to avoid the spurious oscillations usually associated with a collocated grid incompressible solution. The mass flux is then updated and a new pressure field is computed using the updated mass flux $\left(m_f^*\right)$.

$$\sum_f \left(\nabla p\cdot\mathbf{n}dS\right)_f = \frac{\sum_f m_f^*}{\Delta t} \tag{9}$$

The pressure is computed from equation (9) using Gauss-Seidel iteration. The pressure field obtained with the provisional velocity field $\left(\mathbf{V}^*\right)$ does not satisfy the continuity equation. An iterative method is used for the convergence of the mass flux m_f to a predetermined tolerance level. In this 'inner iteration', the mass flux is corrected using the pressure field just obtained. A new provisional velocity field is then recalculated using the equation (7) with the pressure term dropped but the new mass flux included. The pressure field is recalculated using the new provisional velocity field. This iterative loop is continued until the mass flux is converged. Finally, the velocity field $\left(u_{iP}^{n+1}\right)$ is computed using the equation (7) with the converged mass flux and pressure.

The boundary conditions used for the solution are as follows. A convective boundary condition is used in the exit plane so that the vortices pass out smoothly. The convective boundary condition is taken as

$$\frac{\partial u_i}{\partial t} + U_c \frac{\partial u_i}{\partial n} = 0 \tag{10}$$

The convection velocity U_c is the average of the velocity distribution at the exit plane. The no-slip boundary condition is satisfied on all solid boundaries. The pressure satisfies the Neumann condition on all boundaries.

Results and Discussions

All the computations reported here are carried out on a computational mesh made up of 58378 triangular elements connecting 29797 vertices. The mesh is adequately refined so that the wake and boundary layers are appropriately resolved. To assess the accuracy of the developed code, the computed results for flow about a circular cylinder in an unconfined domain are compared with the solution due to Zhou et al. [1999]. The comparisons at Reynolds numbers 100 and 200 are presented in Table 1. The Strouhal number $\left(St = f_S^* D/V\right)$, the mean drag coefficient and the RMS lift coefficient agree quite well with the values reported. The parameter f_S^* denotes the vortex shedding frequency of the rigid cylinder.

Table 1: Comparison of computed results for an unconfined cylinder

	Re	St	C_{dmean}	C_{lrms}
Zhou et al. (1999)	100	0.163	1.475	0.219
Present simulation	100	0.165	1.451	0.226
Zhou et al. (1999)	200	0.192	1.320	-
Present simulation	200	0.195	1.337	0.474

The effects of the imposed transverse magnetic field are studied for various Reynolds numbers in the range $50 \le \mathrm{Re} \le 250$ with varying magnetic field strength. However, typical results for flows at Reynolds numbers 50 and 250 are presented here for brevity. The streamlines of the flow at Reynolds number 50 subjected to various imposed transverse magnetic fields are shown in Figure 2(a-c). The flow is steady and symmetric about the centerline at all Hartmann numbers. With zero Hartmann number, the flow at Re = 50 is time-independent with a pair of counter-rotating vortices attached to the rear face of the cylinder forming a closed wake. The streamlines in the figures clearly show that the flow remain steady with increasing Hartmann number but the separation zone characterized by the wake length reduces as the Hartmann number increases. This can be explained by the fact that an imposed magnetic field in the transverse direction of the flow of a conducting fluid induces Lorentz force in the upstream direction. This force has a tendency to suppress the diffusion of vortices out of the wall and, hence, shortens the wake. Figure 3(a-c) shows the temporal variation of the lift coefficient at different Hartmann numbers for Reynolds number of 50. The figure shows that the average lift coefficient is constant at zero after an initial transient period. The time histories of the lift coefficient at different Hartmann numbers confirm that in each case the flow has reached a time-independent steady state and is symmetric about the

centerline. However, the time to reach the steady state decreases with increase in the Hartmann number. The time variation of the average drag coefficient at Reynolds number 50 with different Hartmann numbers is shown in Figure 4(a-c). The drag coefficient also confirms the steady nature of the flow. These results show that the steady state is reached quicker as the magnetic field strength increases. In addition, it is observed that the average drag coefficient increases marginally with increase in Hartmann number. It may be attributed to the fact that the increased amount of Lorentz force increases the pressure drop to keep on the flow with fixed discharge. This increase in pressure drop due to significant increase in pressure on the front contributes to the increase in the pressure drag on the body.

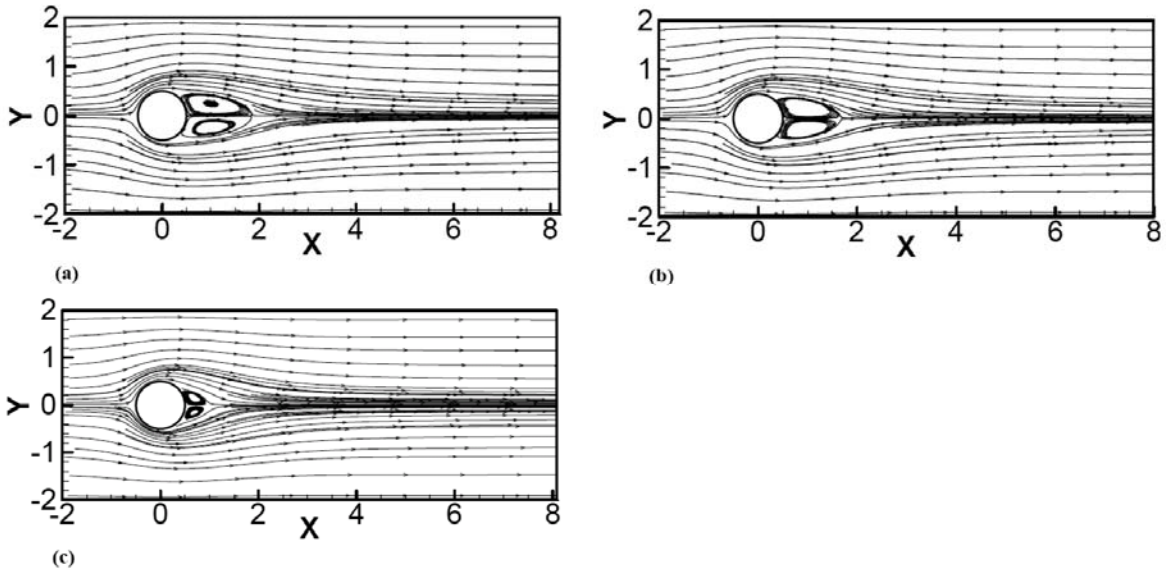

Figure 2. Streamlines at Re = 50 with transverse magnetic field
(a) H_m = 0.0, (b) H_m = 1.0 and (c) H_m = 3.0

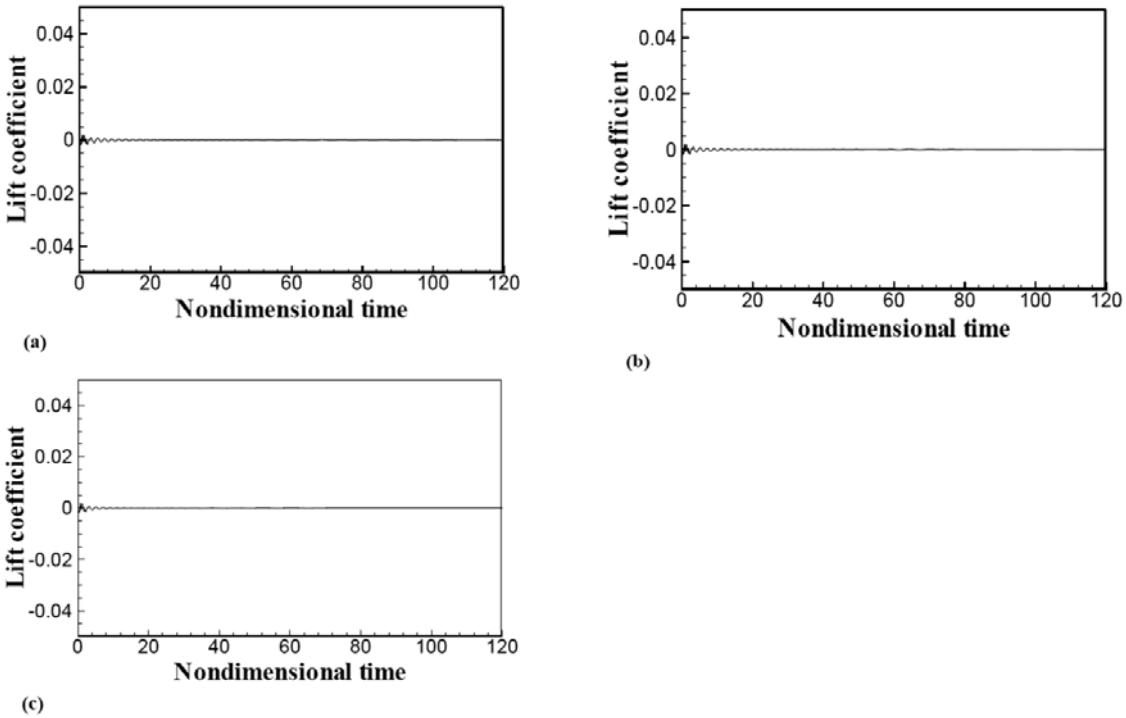

Figure 3. Temporal growth of lift coefficient at Re = 50
(a) H_m = 0.0, (b) H_m = 1.0 and (c) H_m = 3.0

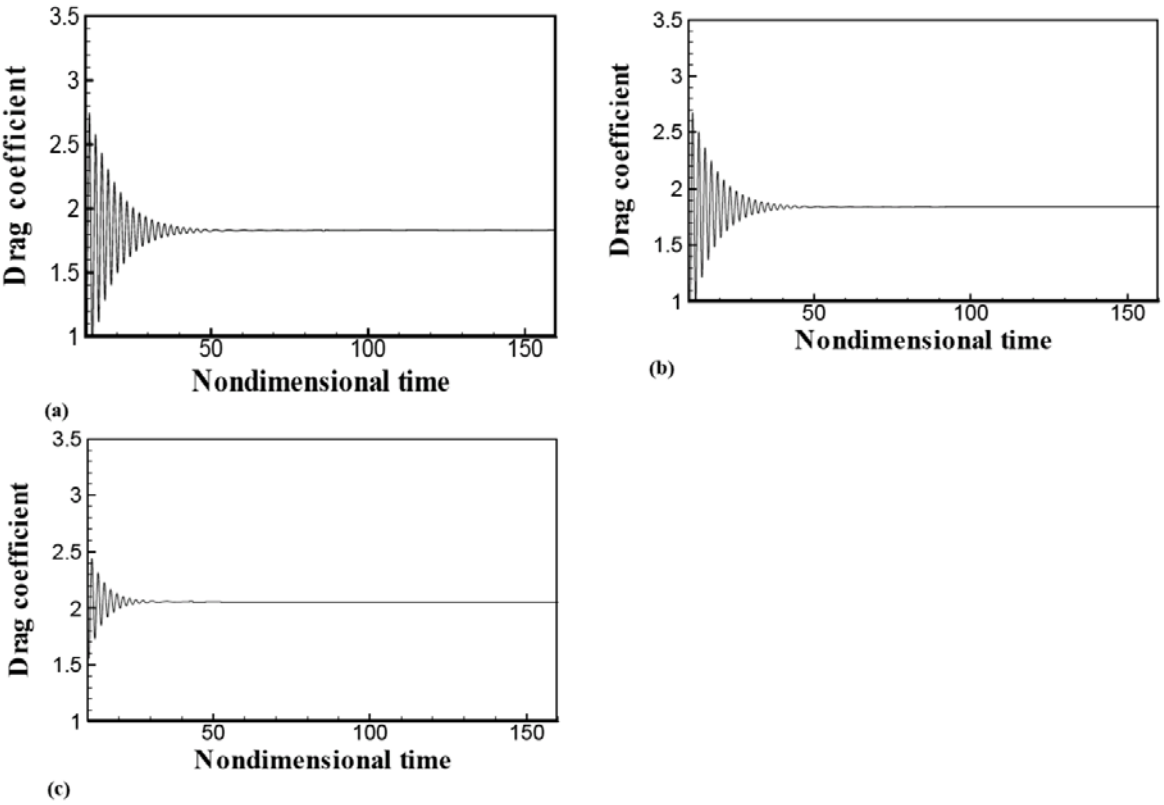

Figure 4. Temporal growth of drag coefficient at Re = 50
(a) H_m = 0.0, (b) H_m = 1.0 and (c) H_m = 3.0

The flow at Re = 250 without an imposed magnetic field is time-dependent with a very long wake due to alternate 'shedding of vortices' from the lower and upper part of the circular cylinder. The instantaneous streamline pattern for this case is shown in Figure 5(a). The streamline patterns for various imposed transverse magnetic fields are shown in Figure 5(a-d). The snapshots of streamlines show that the flow remains unsteady with periodic vortex shedding up to a certain Hartmann number beyond which the flow become steady with a closed wake and with further increase in Hartmann number the wake length decreases. Since the strength of the shed vortices falls with the gradual increase of the Hartmann number, the flow asymmetry and the amplitude of the lift coefficient decrease as shown in Figure 6(a-b). With further increase of the Hartmann number the vortex shedding process is eliminated and the flows as presented in Figure 5(c-d) are steady, symmetric and characterized by closed wakes. The cylinder is subjected to zero lift, shown in Figure 6 (c-d), as in very low Reynolds number flow. The evolution of the drag coefficient at different Hartmann numbers presented in Figure 7(a-d) also reflects the change in the flow regime. There is considerable fluctuation in the drag coefficient when no magnetic force is acting but the fluctuation is significantly reduced at H_m = 2.0. The flow remains unsteady at H_m = 2.0 but the amplitude of oscillations of both the lift and drag coefficient has considerably decreased compared to the 'no imposed magnetic field'. This implies that the strength of the shed vortices and the resulting flow asymmetry that essentially generates the lift has decreased. This feature of the flow has also been observed in the streamline plots in Figure 5(a-d). With stronger magnetic field corresponding to H_m = 5.5, the periodic vortex shedding and the consequent unsteadiness and flow asymmetry are eliminated, as evident from the lift and drag coefficient histories in Figures 6(c) and 7(c) respectively. The same physical process that shortens the wake also weakens the shed vortices and finally suppresses the shedding if the Lorentz force is strong enough. It can be concluded that the amplitude of cross flow vibration will reduce significantly for an elastically mounted cylinder with increase in Hartmann number and the vibration can be eliminated if the Hartmann number is increased appropriately. With further increase in the Hartmann number, the length of the attached wake decreases and the drag coefficient slightly increases. The change in the average drag coefficient due to the change in magnetic field strength shows a very striking result. It is observed that the average drag coefficient decreases marginally with increase in the Hartmann number as long as the flow remains unsteady with alternate periodic vortex shedding. This marginal drop in drag force can be attributed to the weakened shed vortices that nullify the effect of increased pressure drop. However, once the flow becomes steady due to sufficiently strong magnetic field the average drag coefficient increases with further increase in Hartmann number due to the increased pressure drop.

The range of minimum Hartmann numbers within which the periodic vortex shedding is completely suppressed and the initial unsteady flow converts to a steady flow at different Reynolds numbers are given in the Table 2. It is seen that the unsteady flow at higher Reynolds numbers need stronger magnetic field to become steady. It is also observed that the threshold or critical Hartmann number for suppressing the shedding of vortices completely is marginally higher for the circular cylinder compared to a square cylinder (Singha et al. 2007). The difference is negligible at the Reynolds number of 150, but increases slowly with increasing Reynolds number. The difference in terms of the actual magnetic strength is still quite small. The most important point, however, is that the shedding can be eliminated in both cases with a relatively weak magnetic field.

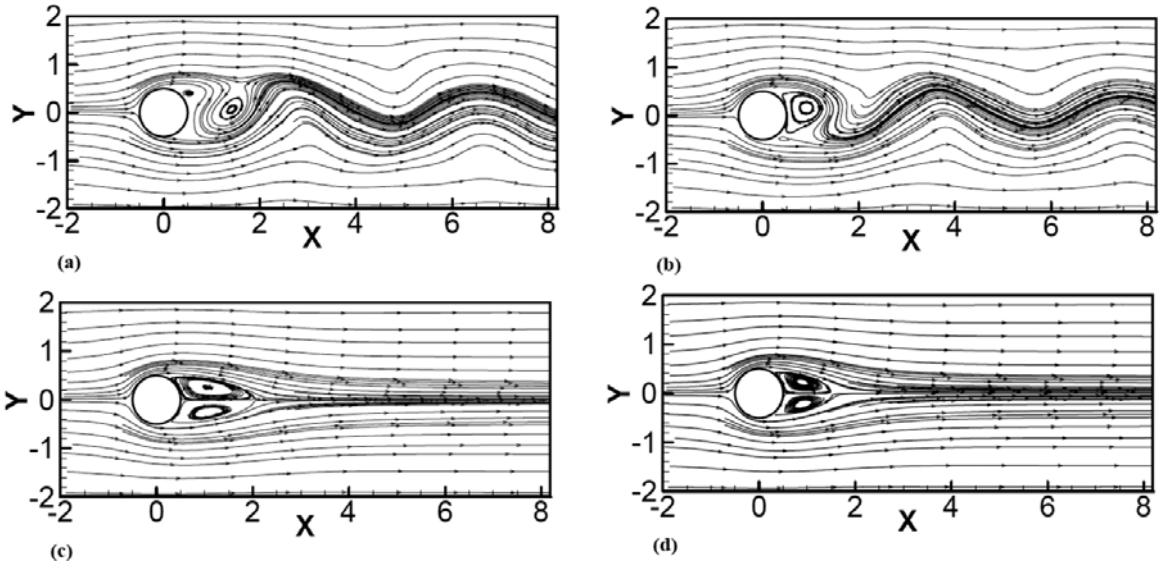

Figure 5. Streamlines at Re = 250 with transverse magnetic field
(a) H_m = 0.0, (b) H_m = 2.0, (c) H_m = 5.5 and (d) H_m = 7.0

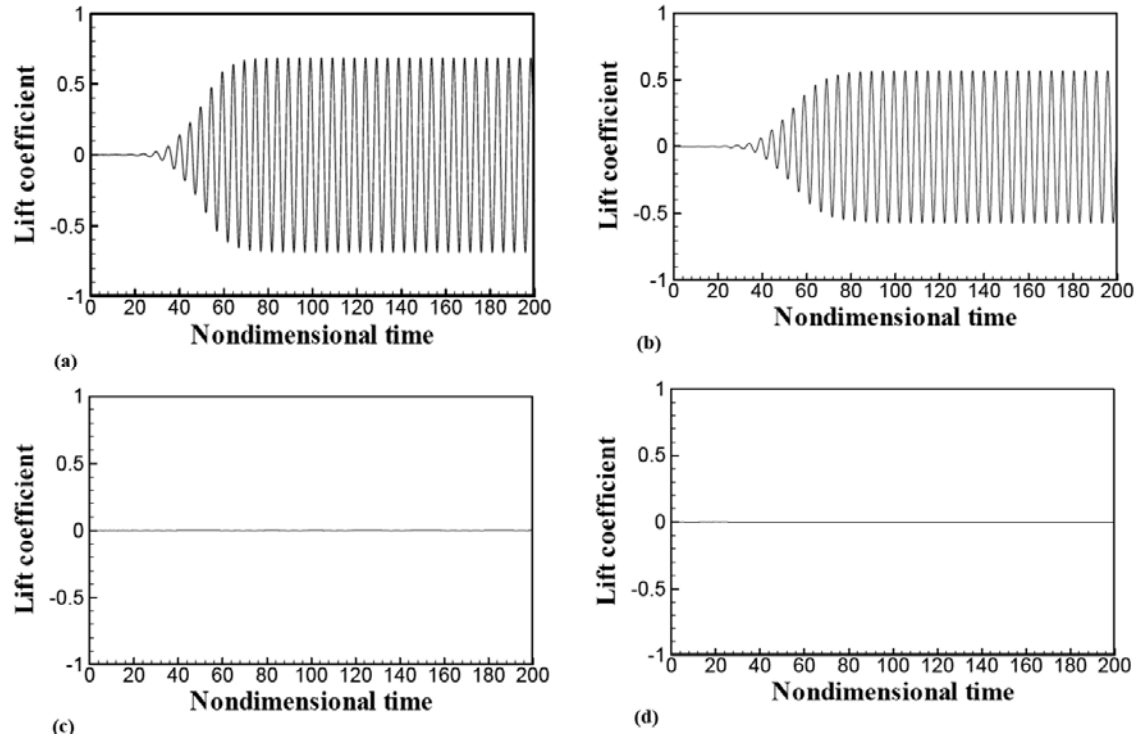

Figure 6. Time history of lift coefficient at Re = 250
(a) H_m = 0.0, (b) H_m = 2.0, (c) H_m = 5.5 and (d) H_m = 7.0

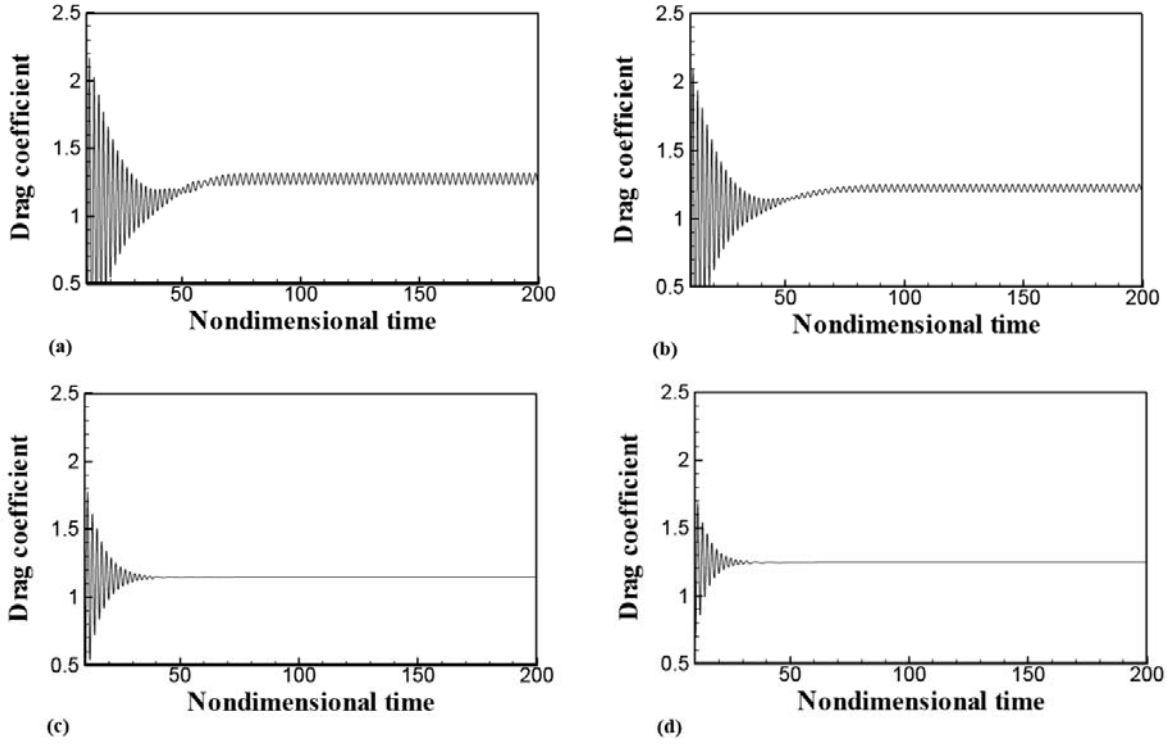

Figure 7. Time history of drag coefficient at Re = 250
(a) H_m = 0.0, (b) H_m = 2.0, (c) H_m = 5.5 and (d) H_m = 7.0

Table 2: Hartmann number required for suppression of vortex shedding

Reynolds Number	Range of H_m	
	Square cylinder (Singha et al. 2007)	Circular cylinder
150	2.0 – 2.5	2.0 – 2.5
200	3.5 – 4.0	4.0 – 4.5
250	4.5 – 5.0	5.0 – 5.5

The instantaneous vorticity contours at different Hartmann numbers for Reynolds number of 250 are presented in Figure 8(a-g). It is already seen that the flow at $\mathrm{Re} = 250$ remains unsteady for $H_m \le 5.0$ but becomes steady in the range $5 < H_m < 5.5$. The vortex patterns confirm the observation. In the unsteady regime, the alternate periodic vortex shedding from the cylinder is evident. However, the arrangement of the vortices in the wake is opposite to the classic Karman vortex-street wake that forms in an unbounded flow. In the unconfined flow, the vortices of negative and positive sign shed off the upper and lower portion of the cylinder respectively and lie above and below the centerline in a staggered vortex array which is the key structure of the Karman vortex-street. The vorticity contours shown in Figure 8(a-f) reveal that as usual the vortices of negative and positive sign shed from the upper and lower portion of the cylinder respectively. However, the arrangement of the vortices is opposite to the classic Karman vortex street at a little distance downstream with regard to their vertical positions. It seems that the opposite-signed vortices associated with the shear layer of the

near wall repel the shed vortices to switch side. Subsequently, the shed vortices attract the same-signed vortices in the shear layer of the other side. The interacting effect of the cylinder wake vortices on the wall boundary layer growth is evident in the vorticity contours shown in the figure. The nearly periodic acceleration and deceleration induced by the wake vortices affects the growth of the wall shear layer downstream of the cylinder to give it an unsteady undulating appearance. These features are essentially associated with the presence of the solid walls as can be concluded from the vorticity contours in Figure 8(a) corresponding to the 'no magnetic field' case. Zovatto and Pedrizzetti [2001] have reported identical vortex structure in the wake of a circular cylinder confined between two parallel plane walls. These features of the confined flow are maintained in the presence of imposed magnetic field below the critical strength. However, with increasing magnetic field strength the interaction greatly reduces as seen in Figure 8(d-f). Finally, the vortex shedding and flow unsteadiness ceases as the Hartmann number reaches the critical value.

Figure 9(a) shows the variation in the length of the attached wake in the steady flow regime with Hartmann number for several Reynolds numbers. It is observed that at a fixed Reynolds number the wake length decreases significantly with increase in Hartmann number. The variation is nearly linear within the selected ranges of the parameters. In this respect the flow behaviour is identical to the flow about a square cylinder (Singha et al., 2007). The variations in Strouhal number with Hartmann number for different Reynolds numbers are presented in Figure 9(b). The imposed magnetic field does not appreciably affect the frequency of vortex shedding in case of flow over a circular cylinder and the Strouhal number remains almost constant for Hartmann numbers below the critical value. This feature of the circular cylinder flow is in contrast with the square cylinder flow where the Strouhal number increases with Hartmann number until the critical value is reached. The increase is marginal at the lower Reynolds numbers but is considerable at the higher Reynolds numbers (Singha et al., 2007).

Figure 10 presents the dependency of the average drag coefficient on the Hartmann number at different Reynolds number. The drag coefficient increases steadily with increasing Hartmann number in the steady flow regime. The increase is initially slow for Hartmann numbers little over the critical value but at higher Hartmann number the increase in drag coefficient is quite rapid. In the unsteady regime, the drag coefficient decreases marginally with increasing magnetic field strength.

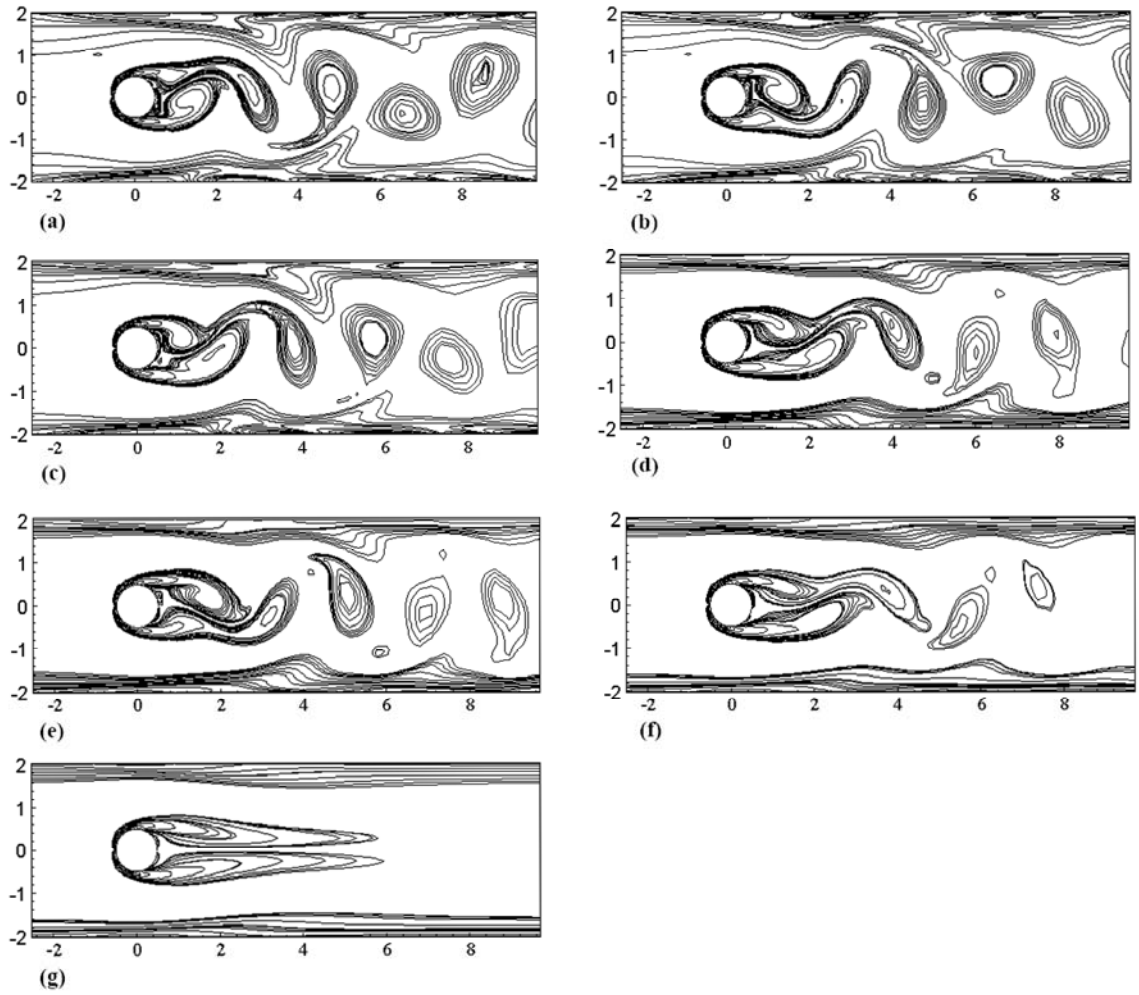

Figure 8. Instantaneous vorticity contours at Re = 250 with transverse magnetic field (a) $H_m = 0$, (b) $H_m = 1.0$, (c) $H_m = 2.0$, (d) $H_m = 3.0$, (e) $H_m = 4.0$, (f) $H_m = 5.0$, (g) $H_m = 5.5$

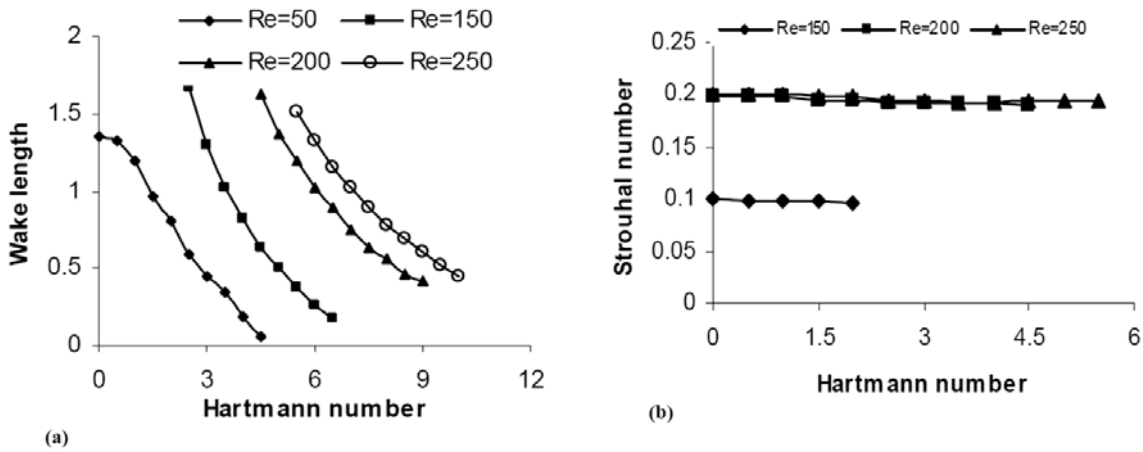

Figure 9. Variation of (a) Wake length and (b) Strouhal number with Hartmann number

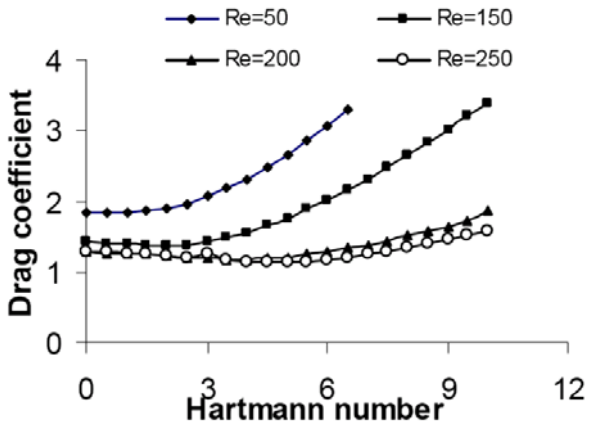

Figure 10. Variation of mean drag coefficient with Hartmann number

Conclusions

Low Reynolds number laminar flows around a confined circular cylinder subjected to an imposed uniform transverse magnetic field are studied using an unstructured collocated grid finite volume implicit incompressible Navier-Stokes solver. The fluid is assumed to have a uniform electrical conductivity. The induced magnetic field is assumed to be negligible in comparison with the imposed magnetic field which is justified for MHD flows at very small magnetic Reynolds numbers. It is observed that in the closed attached wake regime of the flow the wake length decreases approximately linearly with increase in Hartmann number. In the periodic wake regime the vortex shedding and unsteadiness reduces as the Hartmann number increases and if a sufficiently strong magnetic field is applied the vortex shedding is suppressed. The limiting Hartmann number at which shedding is suppressed increases with Reynolds number. The limiting Hartmann number is marginally greater for circular cylinder flows compared to square cylinder flows. The difference increases with Reynolds number. The interaction between the vortices shed from the cylinder and wall shear layer is also found to decrease with increasing Hartmann number. With increasing Hartmann number the drag coefficient is found to decrease marginally in the unsteady flow regime but to increase considerably in the steady flow regime. At a Reynolds number of 150 the mean drag coefficient falls by nearly 4% as the Hartmann number increases from 0.0 to 2.5 and subsequently increases by 48% at Hartmann number of 6.5. The drag coefficient increases more rapidly at higher Hartmann numbers. The amplitude of the periodic lift coefficient decreases with increase in Hartman number and falls to zero at the limiting Hartmann number. It is seen that the Strouhal number at a fixed Reynolds number is insensitive to the change in Hartmann number as long as the flow remains unsteady. This characteristic of the flow about circular cylinder is in contrast to the flow about square cylinder.

References

1. Bramley JS. Magnetohydrodynamic flow past a circular cylinder. *Journal of Applied Mathematics and Physics ZAMP* 1974; 25 (3), 409-416.
2. Bramley JS. Magnetohydrodynamic flow past a circular cylinder II. *Journal of Applied Mathematics and Physics ZAMP* 1974; 26 (2), 203-209.
3. Gerbeth G, Thess A, Marty P. Theoretical study of the MHD flow around a cylinder in crossed electric and magnetic fields, *Europ. Journ. of Mech.*, 9, #3, p.239-257, 1990.
4. Josserand J, Marty Ph, Alemany A. Pressure and drag measurements on a cylinder in a liquid metal flow with an aligned magnetic field. *Fluid Dynamic Research* 1993; 11, 107–117.
5. Mutschke G, Shatrov V, Gerbeth G. Cylinder wake control by magnetic fields in liquid metal flows. *Experimental Thermal and Fluid Science* 1998; 16, 92-99.
6. Midya C, Layek GC, Gupta AS, Mahapatra RT. Magnetohydrodynamic viscous flow separation in a channel with constriction. *ASME Journal of Fluids Engineering* 2003, 125, 952-962.
7. Sekhar TVS, Sivakumar R, Ravikumar TVR. Flow around a circular cylinder in an external magnetic field at high Reynolds numbers, *International Journal of Numerical Methods for Heat & Fluid Flow*, 16, 740-759, 2006.
8. Singha S, Sinhamahapatra KP, Mukherjea SK. Control of vortex shedding from a bluff body using imposed magnetic field. *ASME Journal of Fluids Engineering* 2007; 129, 517-523.
9. Knaepen B, Kassinos SC, Carati D. MHD turbulence at moderate magnetic Reynolds number. *Journal of Fluid Mech.*, 513, 199-220, 2004.
10. Kassinos SC, Carati D, Knaepen B. The transport of a passive scalar in MHD turbulence subjected to mean shear and frame rotation. *Physics of Fluids*, 19, 015105-(1-23), 2007, DOI: 10.1063/1.2409732
11. Saaris I, Kassinos SC, Carati D. Large-Eddy Simulations of the turbulent Hartmann flow close to the transitional regime. *Physics of Fluids*, 19, 085109-(1-9), 2007, DOI: 10.1063/1.2757710.
12. Zovatto L, Pedrizzetti G. Flow about a circular cylinder between parallel walls. *Journal of Fluid Mechanics* 2001; 440, 1-25.
13. Shercliff JA. *A Textbook of Magnetohydrodynamics*. Pergamon Press, New York, 1965.
14. Rhie CM, Chow WL. A numerical study of the turbulent flow past an isolated airfoil with trailing edge separation. *AIAA Journal* 1983; 21, 1525 –1532.
15. Leonard BP. A stable and accurate convective modeling procedure based on quadratic upstream interpolation. *Computational Methods in Applied Mechanics and Engineering* 1979; 19, 59-98.
16. Holmes DG, Connel SD. Solution of 2D Navier-Stokes equations on unstructured adaptive grids. *AIAA paper 89-1932-CP* 1989.
17. Zhou CY, So RMC, Lam K. Vortex-induced vibration of an elastic circular cylinder. *Journal of Fluids and Structures* 1999; 13**,** 165-189.

Table 1: Comparison of computed results for an unconfined cylinder

	Re	St	C_{dmean}	C_{lrms}
Zhou et al. (1999)	100	0.163	1.475	0.219
Present simulation	100	0.165	1.451	0.226
Zhou et al. (1999)	200	0.192	1.320	-
Present simulation	200	0.195	1.337	0.474

Table 2: Hartmann number required for suppression of vortex shedding

Reynolds Number	Range of H_m	
	Square cylinder (Singha et al. 2007)	Circular cylinder
150	2.0 – 2.5	2.0 – 2.5
200	3.5 – 4.0	4.0 – 4.5
250	4.5 – 5.0	5.0 – 5.5

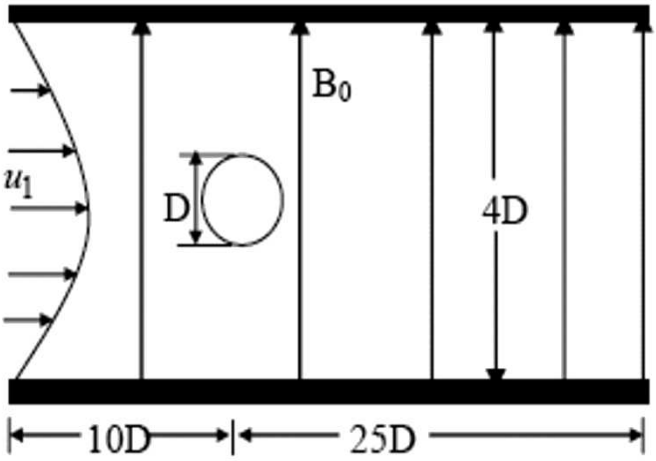

Figure 1. The computational flow domain

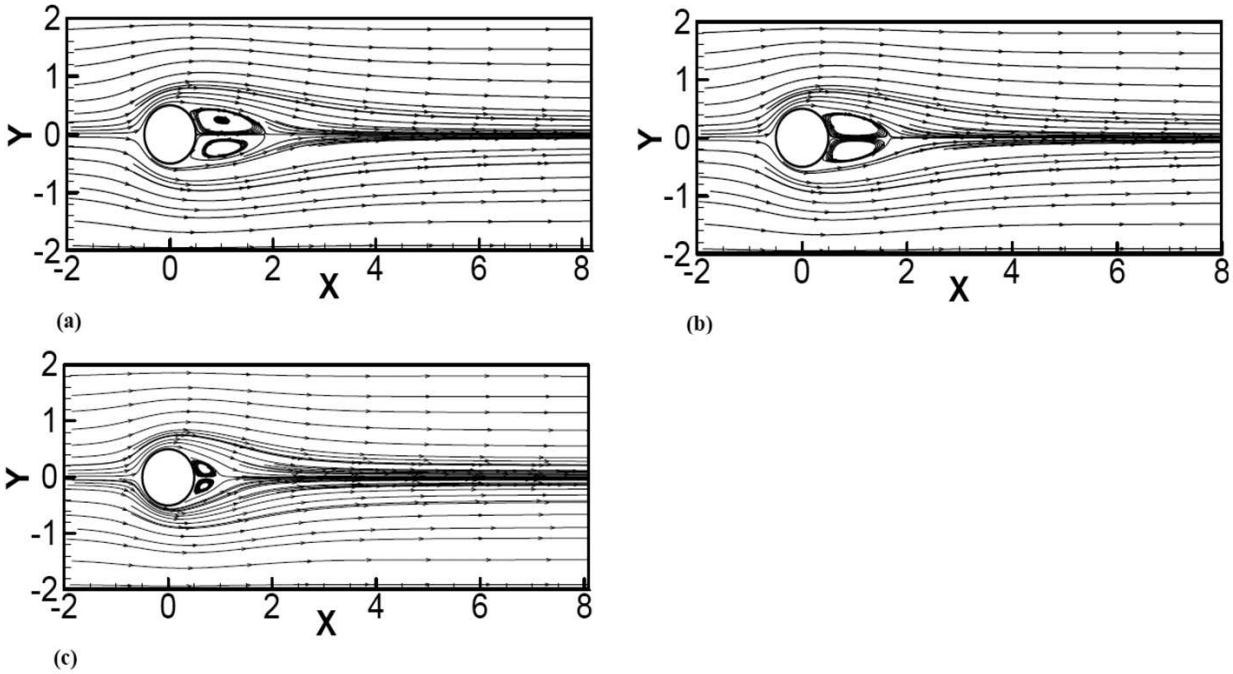

Figure 2. Streamlines at Re = 50 with transverse magnetic field
(a) H_m = 0.0, (b) H_m = 1.0 and (c) H_m = 3.0

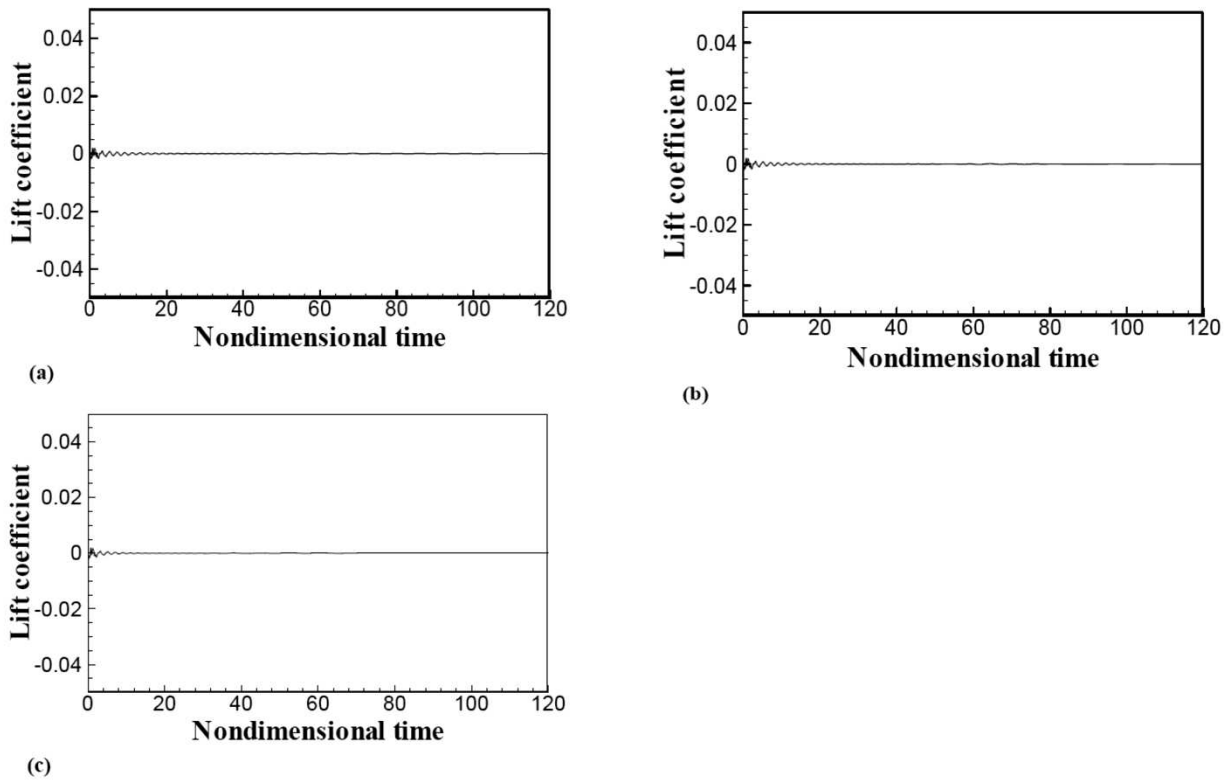

Figure 3. Temporal growth of lift coefficient at Re = 50
(a) $H_m = 0.0$, (b) $H_m = 1.0$ and (c) $H_m = 3.0$

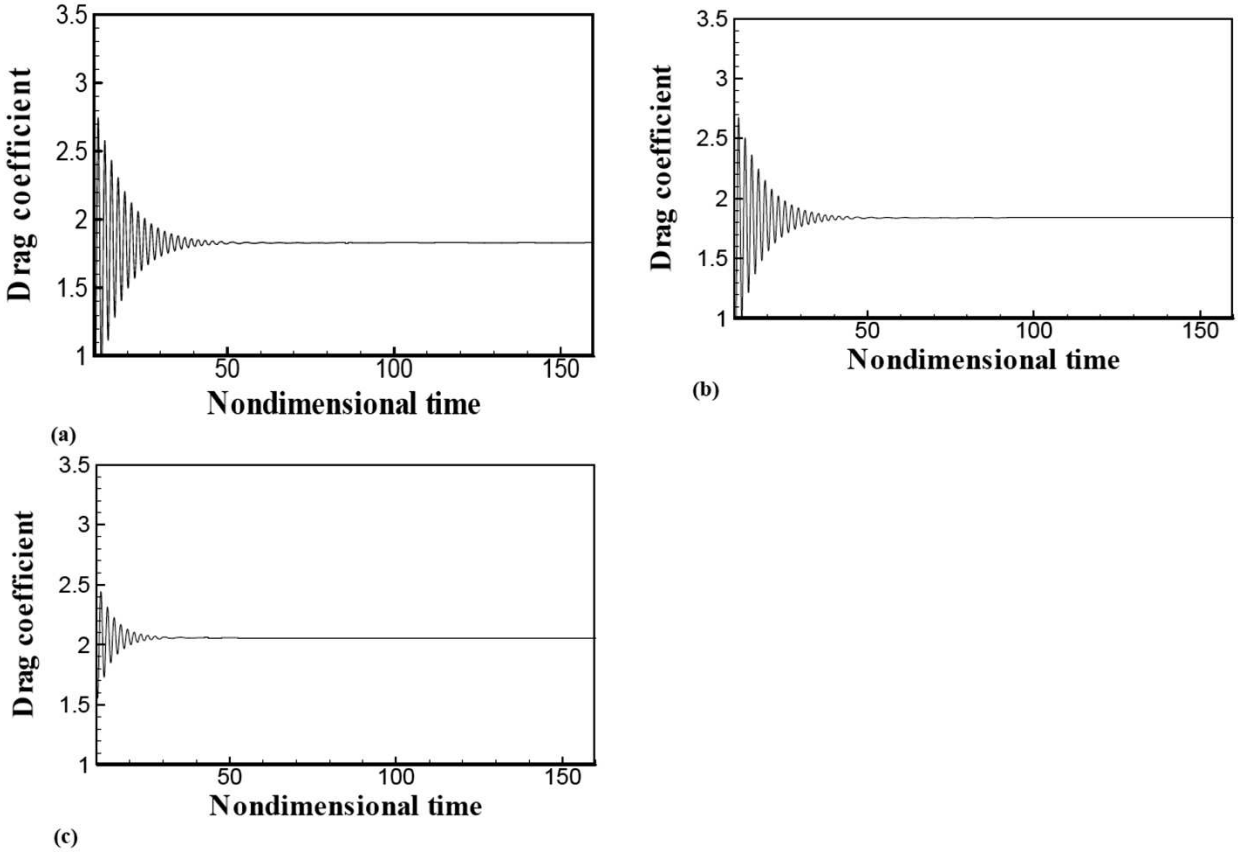

Figure 4. Temporal growth of drag coefficient at Re = 50
(a) H_m = 0.0, (b) H_m = 1.0 and (c) H_m = 3.0

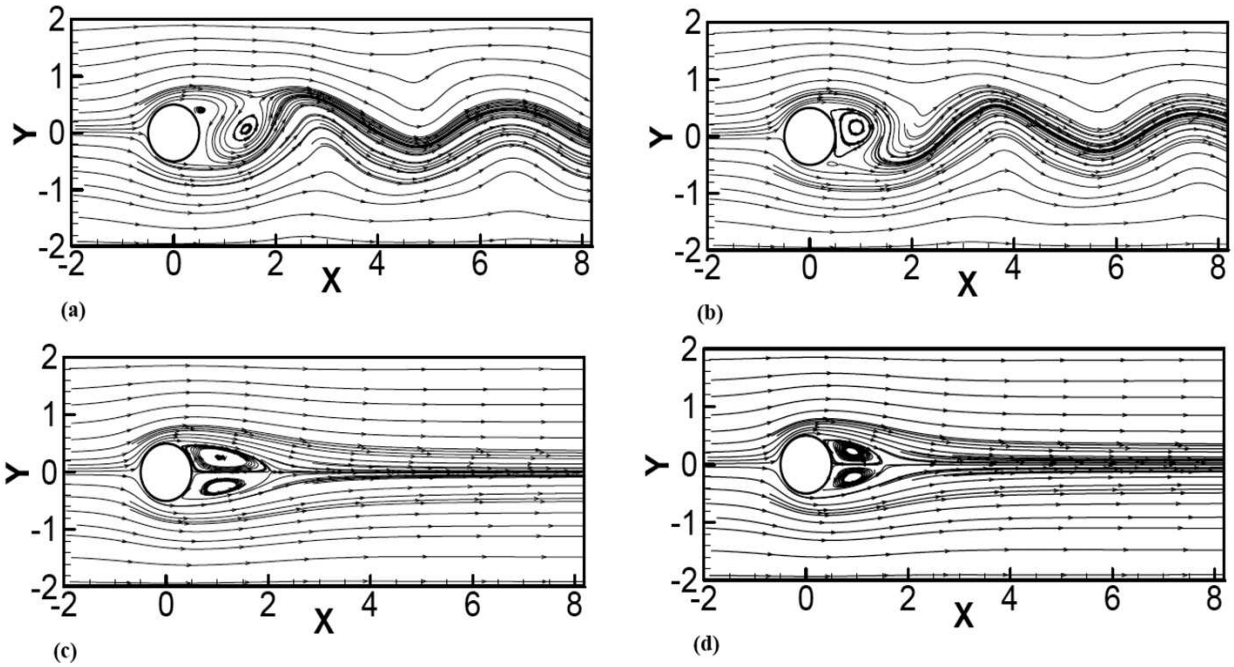

Figure 5. Streamlines at Re = 250 with transverse magnetic field
(a) $H_m = 0.0$, (b) $H_m = 2.0$, (c) $H_m = 5.5$ and (d) $H_m = 7.0$

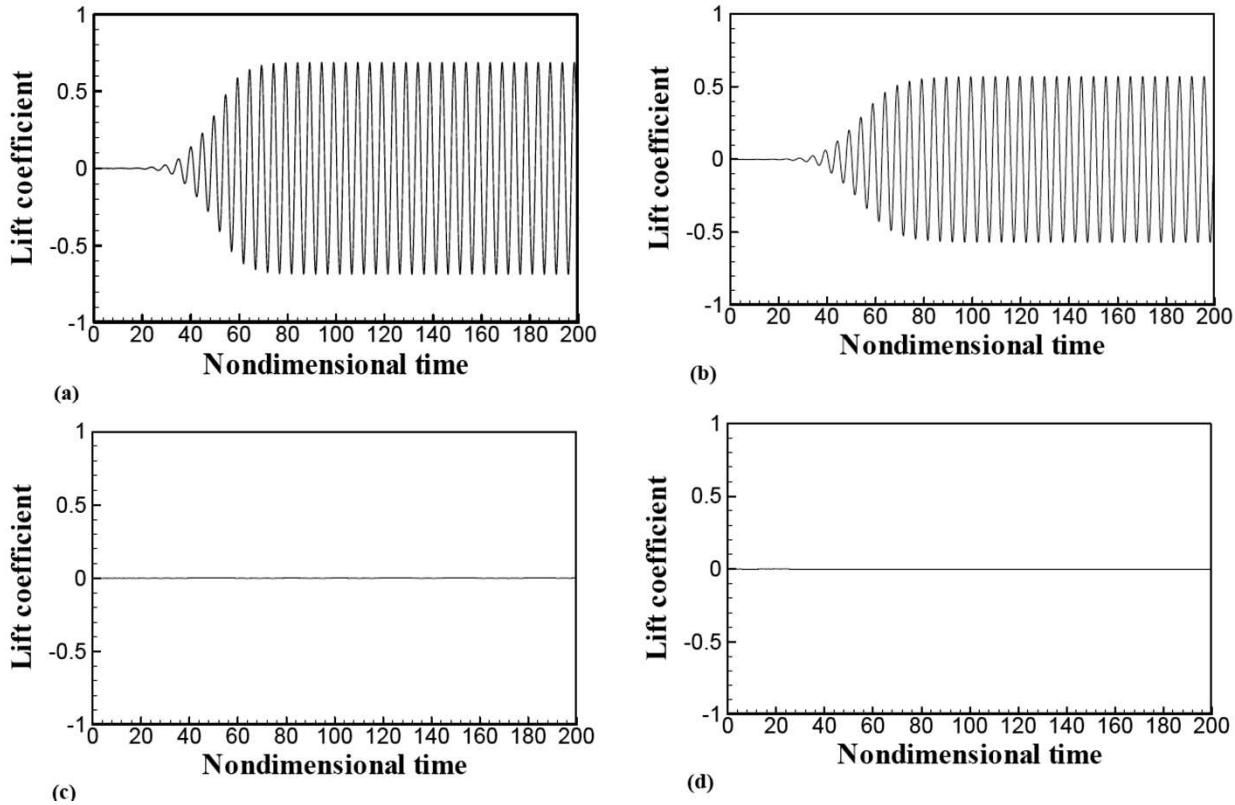

Figure 6. Time history of lift coefficient at Re = 250
(a) H_m = 0.0, (b) H_m = 2.0, (c) H_m = 5.5 and (d) H_m = 7.0

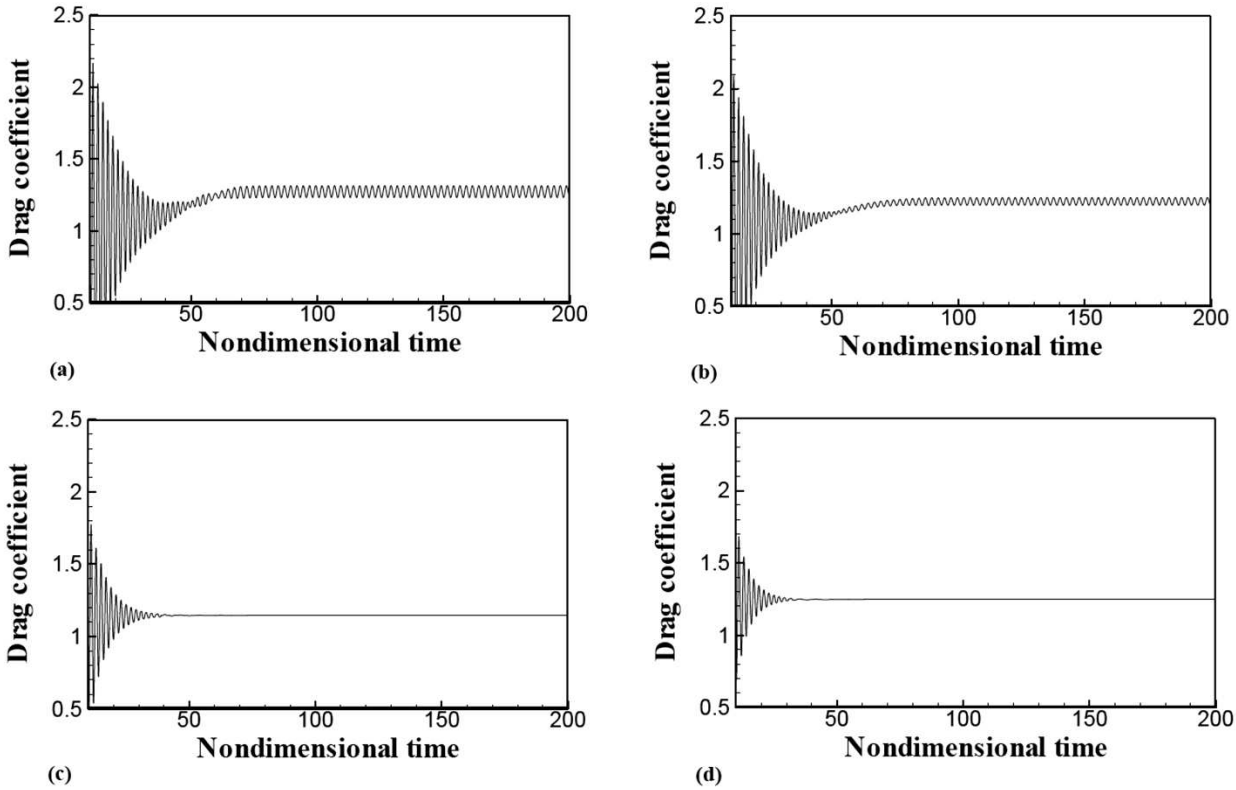

Figure 7. Time history of drag coefficient at Re = 250
(a) H_m = 0.0, (b) H_m = 2.0, (c) H_m = 5.5 and (d) H_m = 7.0

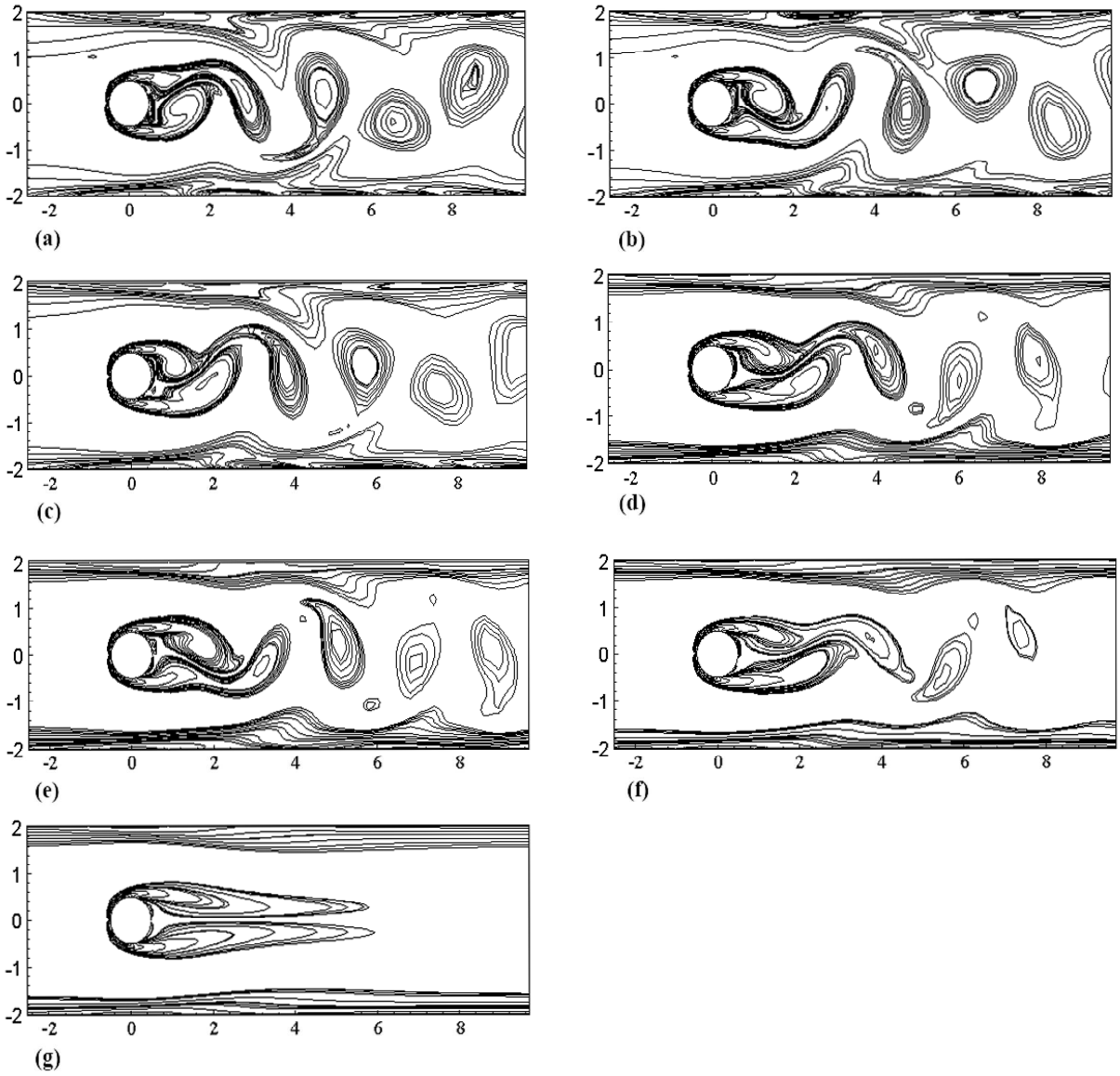

Figure 8. Instantaneous vorticity contours at Re = 250 with transverse magnetic field
(a) $H_m = 0$, (b) $H_m = 1.0$, (c) $H_m = 2.0$, (d) $H_m = 3.0$, (e) $H_m = 4.0$, (f) $H_m = 5.0$, (g) $H_m = 5.5$

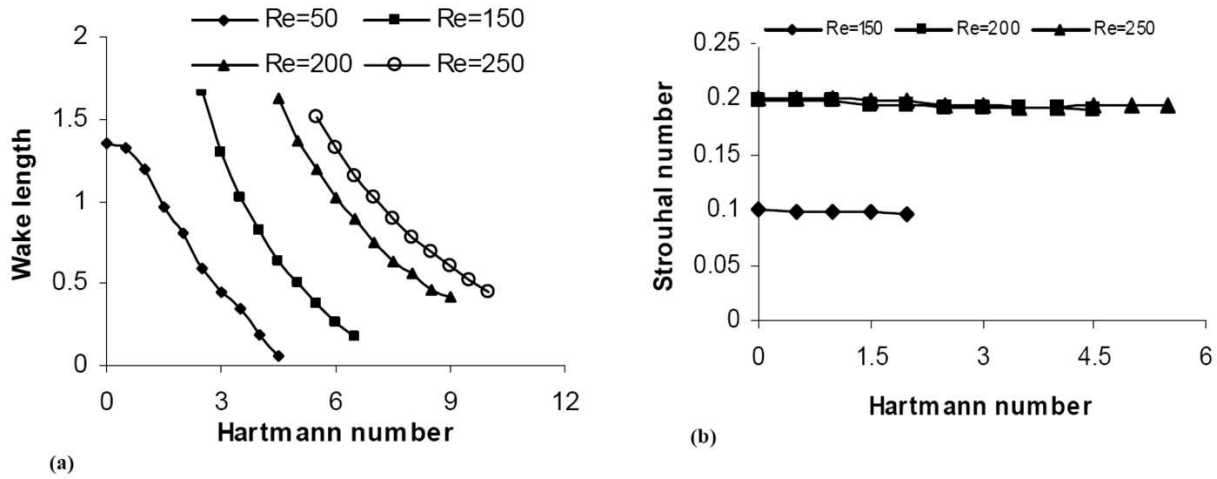

Figure 9. Variation of (a) Wake length and (b) Strouhal number with Hartmann number

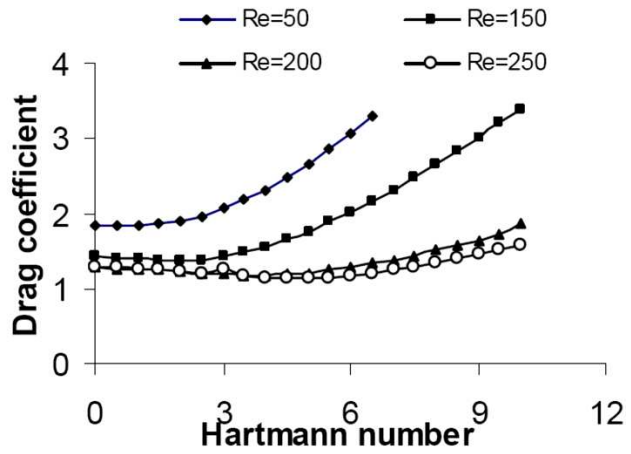

Figure 10. Variation of mean drag coefficient with Hartmann number

Control of Vortex Shedding from a Circular Cylinder using Imposed Transverse Magnetic Field

Sintu Singha and K. P. Sinhamahapatra
Department of Aerospace Engineering, IIT Kharagpur
Kharagpur 721302, India

Abstract

Purpose - The flow of a conducting fluid past a circular cylinder placed centrally in a channel subjected to an imposed transverse magnetic field has been simulated to study the effect of a magnetic field on vortex shedding at different Reynolds numbers varying from 50 to 250.
Design/Methodology/Approach - The two-dimensional incompressible laminar viscous flow equations are solved using a second-order implicit unstructured collocated grid finite volume method.
Findings - An imposed transverse magnetic field markedly reduces the unsteady lift amplitude indicating a reduction in the strength of the shed vortices. It is observed, that the periodic vortex shedding at the higher Reynolds numbers can be completely suppressed if a sufficiently strong magnetic field is imposed. The required magnetic field strength to suppress shedding increases with Reynolds number. The simulation shows that the separated zone behind the cylinder in a steady flow is reduced as the magnetic field strength is increased.
Originality/Value - Due attention is given to resolve and study the unsteady cylinder wake and its interaction with the shear-layer on the channel wall in the presence of a magnetic field. A critical value of the Hartmann number for complete suppression of the shedding at a given Reynolds number is found.

Keywords: transverse magnetic field, Hartmann number, vortex shedding, wake, circular cylinder, separation

Introduction

The flow over a circular cylindrical body is a common phenomenon in many engineering applications. The flow is essentially unsteady except at very low Reynolds numbers less than about 50. The steady flow at a low Reynolds number is characterized by steady separation and a closed near wake of recirculating flow. At relatively higher Reynolds numbers, the relevant unsteady flows are characterized by the periodic shedding of vortices and unsteady separated vortex wake. The unsteady flow exerts fluctuating forces on the immersed bodies. The fluctuating forces on the bluff body may cause the body to vibrate, which may be severe for a range of natural frequency to the vortex shedding frequency ratio, particularly if the mass ratio and damping are low. The control of such 'flow-induced vibration' can be achieved if the vortex shedding and/or the size of the separated zone behind the body are controlled. An imposed transverse magnetic field does the job satisfactorily when the fluid is electrically conducting. The use of magnetic field in the cross-stream direction is a novel method of controlling the separated zone behind the body, which in turn helps to reduce or

eliminate the periodic vortex shedding and the resulting flow-induced vibration in a conducting fluid. Bramley [1974a, 1974b] studied the steady two-dimensional incompressible MHD flow past a circular cylinder with an applied magnetic field parallel to the main flow using analytical and numerical methods. It was observed that with an applied magnetic field the flow remained attached to the cylinder longer and in some cases did not separate until the rear stagnation point. Gerbeth et al. [1990] studied steady unidirectional MHD flow around a cylinder driven by crossed electric and magnetic fields analytically using series solution. Josserand et al. [1993] studied the effect of an aligned magnetic field in the flow of a liquid metal past a cylinder and observed that the magnetic field could reduce the drag on the cylinder and the Karman street behind the cylinder was suppressed for a sufficient value of the magnetic field. Mutschke et al. [1998] studied the controlling influence of external magnetic field on the wake instabilities in the flow of an electrically conducting fluid around a circular cylinder. Midya et al. [2003] investigated the magnetohydrodynamic effect on viscous flow in a channel with constriction. It was observed that the transverse magnetic field reduced the size of the separated zone downstream of the constriction and the separation could be eliminated with a large magnetic field. The wall shear stress, however, increased with the strength of the imposed magnetic field. Sekhar et al. [2006] investigated laminar flow past a circular cylinder subjected to inline magnetic field and observed that parallel magnetic field reduced the wake length. Singha et al. [2007] studied the effect of an applied transverse magnetic field on steady as well as periodic vortex-shedding flow around a square cylinder using an explicit staggered grid finite difference method. Recently Knaepen et al. [2004], Kassinos et al. [2007], Sarris et al. [2007] have studied the structure of MHD turbulence and transport processes in MHD turbulent flows under different conditions using LES and DNS techniques.

In the present work, the incompressible viscous flow of an electrically conducting fluid around a circular cylinder confined symmetrically between two parallel walls in the presence of a uniform transverse magnetic field is studied numerically. The incompressible Navier-Stokes equations are solved using an unstructured collocated grid finite volume method. The solution is advanced in time using a second-order implicit scheme. The study is performed at several Reynolds numbers over a range of magnetic-field strength expressed in terms of the nondimensional Hartmann number. The study shows that the separated wake length decreases with the increase in magnetic field for steady flow cases. The imposed magnetic field reduces the strength of the shed vortices and, hence, reduces the flow asymmetry and lift amplitude in unsteady flows at higher Reynolds numbers. Moreover, the unsteady flows at higher Reynolds numbers can be made steady when the applied magnetic field is sufficiently strong.

Configuration and Numerical Method

The configuration considered is a two dimensional incompressible viscous flow of electrically conducting fluid with constant conductivity σ and density ρ around a circular cylinder of diameter D placed symmetrically between two flat plates as in Figure 1. A uniform magnetic field (B_0) is imposed along the cross-flow direction. The distance between the two plane walls (H) is $4D$. A parabolic streamwise velocity $u_1 = V\left[1-4\left(\frac{y}{H}\right)^2\right]$ is specified at the inlet, where V is the centerline velocity. A plane solid wall near a circular cylinder can suppress the vortex shedding from the cylinder if the gap between them is less than a critical value corresponding to the Reynolds number (Zovatto and Pedrizetti, 2001).

However, a gap space of $1.5D$ corresponding to the channel height of $4D$ is well above the critical height for suppression of the shedding due to wall influence for $\mathrm{Re} \geq 100$.

Due to magnetohydrodynamic interactions, an induced electric field E_z is produced in the direction perpendicular to the plane of the flow, which in turn produces an induced magnetic field in the streamwise direction. It is assumed that the flows considered are of very small magnetic Reynolds number $\mathrm{Re}_m (= \mu\sigma VD$, where V is the characteristic velocity and μ is the permeability) and, hence, the induced magnetic field is negligible so that there is no distortion in the imposed magnetic field (Shercliff, 1965). It is also assumed that the magnetic field is not distorted near the body due to the differences in permeability and conductivity between the solid body and the conducting fluid. Thus, a short-circuited situation is assumed as if the induced current is taken through a stationary closed loop made of perfect conductor lying in the direction perpendicular to the stream. Consequently, the induced electric field (E_z) becomes zero (Shercliff, 1965) and a net current $\sigma B_0 Q$ flows normal to the plane of the flow, where Q is the fluid volume flow rate. It is further assumed that the electric field due to the polarization of charges is negligible. An elegant justification for these assumptions is given by Midya et al. [2003] for the flow of a conducting fluid in a channel with constriction. The presence of a body in the flow, which usually will have a different conductivity, may reduce the accuracy of some of the assumptions. The induced magnetic and electric fields will alter the current flow and the current continuity needs to be taken in to account for better accuracy. However, when the conductivities of the flowing fluid and the cylinder material are nearly of the same order of magnitude and the Hartmann number is small, the induced electric and magnetic fields will not be large enough to have significant effect on the overall flow behavior. With this assumption, the current continuity is not considered in the present study and it is felt that the solution will be able to capture the dominant features of the flow both qualitatively and quantitatively. With the consideration of the Lorentz forces due to the external magnetic field and the assumptions stated above, the governing equations for two-dimensional flows in their nondimensional form are given by

$$\frac{\partial u_i}{\partial x_i} = 0 \tag{1}$$

$$\frac{\partial u_i}{\partial t} + \frac{\partial}{\partial x_j}(u_j u_i) = -\frac{\partial p}{\partial x_i} + \frac{1}{\mathrm{Re}}\frac{\partial^2 u_i}{\partial x_j \partial x_j} - \frac{H_m^2}{\mathrm{Re}} K_i u_i \tag{2}$$

In equation (2), $K_1 = 1$, $K_2 = 1$ and Re is the Reynolds number VD/υ with υ being the kinematic viscosity. The characteristic velocity V is taken as the centerline inflow velocity and the Hartmann number (H_m) is defined as $H_m = B_0 D\sqrt{\sigma/\rho\upsilon}$.

The governing equations (1) and (2) are numerically solved using an unstructured cell-centered collocated grid finite volume method. Integrated over a small control volume, which in this case is a triangular cell of the mesh, the equations can be written as

$$\oint_S \mathbf{V} \cdot \hat{\mathbf{n}} dS = 0 \tag{3}$$

$$\frac{\partial}{\partial t}\int_{\Omega} u_i d\Omega + \iint_S u_i \mathbf{V}\cdot\hat{\mathbf{n}} dS = -\iint_S p n_i dS + \frac{1}{\mathrm{Re}}\iint_S \nabla u_i \cdot \hat{\mathbf{n}} dS - \frac{H_m^2}{\mathrm{Re}}\int_{\Omega} K_i u_i d\Omega \tag{4}$$

where $\mathbf{V}$ is the velocity vector of the fluid element, Ω and S denote the nondimensional control volume and the bounding surface of the control volume respectively. The unit vector normal to the surface S is $\hat{\mathbf{n}}$ and n_i denotes the Cartesian component of the unit normal vector.

The convective terms in the momentum equation for a cell are computed as the sum of fluxes across the three faces where the flux across each face is computed as a product of the outward mass flux and the appropriate cell face velocity component. The velocity on a face is obtained using a quadratic upwind interpolation (Leonard, 1979) from the velocity at three points. Two of these three points are the cell centers on either side of the face and the third point is the projection of the distant vertex of the upstream triangle on the line joining the two cell centers.

The diffusive terms in the momentum equation integrated over a triangular control volume is expressed in the following generic form:

$$F_{ij}^{v} = \int_{\Omega} \frac{\partial}{\partial x_i}\left(\frac{\partial \phi}{\partial x_j}\right) d\Omega \qquad i, j = 1, 2;$$

$$= \iint_S \left(\frac{\partial \phi}{\partial x_j}\right) n_i dS \qquad \approx \sum_{k=1}^{3} \frac{\partial \phi}{\partial x_{jk}} n_{ik} dS_k \,, \tag{5}$$

The gradients along the face of a control volume are computed using the values of the variable at the two adjacent cell centers and at the two terminating vertices of the face. The value of the variable ϕ at a vertex of the face is obtained by an interpolation from the cell-centered values of the surrounding cells using the linearity-preserving Laplacian due to Holmes and Connel [1989]. The procedure provides the diffusive flux terms for a cell with center P in terms of the variable at P and at the center of all the neighboring cells shared by the vertices of the cell P.

$$F_{ij}^{v} = a_P \phi_P + \sum_{m \neq P}^{N_1} c_m \phi_m + \sum_{m \neq P}^{N_2} d_m \phi_m + \sum_{m \neq P}^{N_3} e_m \phi_m \tag{6}$$

where N_1, N_2, N_3 are the number of cells connected to the three vertices of the triangular cell P.

The source term in the momentum equation representing the Lorentz force is discretized using the cell-centered variables and the cell volume. The solution is advanced in time using the implicit Crank-Nicolson scheme. The discretized equation is written in the form

$$\frac{u_{iP}^{n+1}-u_{iP}^{n}}{\Delta t}+\frac{1}{2}\left(\sum_f m_f^{n+1}u_{if}^{n+1}+\sum_f m_f^{n}u_{if}^{n}\right)=-\sum_f p_f^{n+1}n_{if}dS_f+\frac{1}{2}\left(\sum_f F_{dif}^{n+1}+\sum_f F_{dif}^{n}\right)+\frac{1}{2}\left(L_{iP}^{n+1}+L_{iP}^{n}\right) \tag{7}$$

where P and f denote the cell-centre and a cell face respectively. F_d is the diffusive flux term, L is the Lorentz force source term and m is mass flux. The index i =1, 2 denotes the streamwise (x) and cross-stream (y) direction respectively. The above equation is solved along with the discretized continuity equation written as

$$\sum_f m_f^{n+1}=0 \tag{8}$$

A provisional velocity field $\left(\mathbf{V}^*\right)$ is first computed using the latest available mass flux and dropping the pressure term from the equation (7). The modified equation is solved using a Gauss-Seidel iterative solver. The provisional velocity field is used to compute the cell face velocities using the Rhie and Chow [1983] interpolation to avoid the spurious oscillations usually associated with a collocated grid incompressible solution. The mass flux is then updated and a new pressure field is computed using the updated mass flux $\left(m_f^*\right)$.

$$\sum_f\left(\nabla p\cdot\mathbf{n}dS\right)_f=\frac{\sum_f m_f^*}{\Delta t} \tag{9}$$

The pressure is computed from equation (9) using Gauss-Seidel iteration. The pressure field obtained with the provisional velocity field $\left(\mathbf{V}^*\right)$ does not satisfy the continuity equation. An iterative method is used for the convergence of the mass flux m_f to a predetermined tolerance level. In this 'inner iteration', the mass flux is corrected using the pressure field just obtained. A new provisional velocity field is then recalculated using the equation (7) with the pressure term dropped but the new mass flux included. The pressure field is recalculated using the new provisional velocity field. This iterative loop is continued until the mass flux is converged. Finally, the velocity field $\left(u_{iP}^{n+1}\right)$ is computed using the equation (7) with the converged mass flux and pressure.

The boundary conditions used for the solution are as follows. A convective boundary condition is used in the exit plane so that the vortices pass out smoothly. The convective boundary condition is taken as

$$\frac{\partial u_i}{\partial n}+U_c\frac{\partial u_i}{\partial n}=0 \tag{10}$$

The convection velocity U_c is the average of the velocity distribution at the exit plane. The no-slip boundary condition is satisfied on all solid boundaries. The pressure satisfies the Neumann condition on all boundaries.

Results and Discussions

All the computations reported here are carried out on a computational mesh made up of 58378 triangular elements connecting 29797 vertices. The mesh is adequately refined so that the wake and boundary layers are appropriately resolved. To assess the accuracy of the developed code, the computed results for flow about a circular cylinder in an unconfined domain are compared with the solution due to Zhou et al. [1999]. The comparisons at Reynolds numbers 100 and 200 are presented in Table 1. The Strouhal number $\left(St = f_S^* D/V\right)$, the mean drag coefficient and the RMS lift coefficient agree quite well with the values reported. The parameter f_S^* denotes the vortex shedding frequency of the rigid cylinder.

The effects of the imposed transverse magnetic field are studied for various Reynolds numbers in the range $50 \le \mathrm{Re} \le 250$ with varying magnetic field strength. However, typical results for flows at Reynolds numbers 50 and 250 are presented here for brevity. The streamlines of the flow at Reynolds number 50 subjected to various imposed transverse magnetic fields are shown in Figure 2(a-c). The flow is steady and symmetric about the centerline at all Hartmann numbers. With zero Hartmann number, the flow at Re = 50 is time-independent with a pair of counter-rotating vortices attached to the rear face of the cylinder forming a closed wake. The streamlines in the figures clearly show that the flow remain steady with increasing Hartmann number but the separation zone characterized by the wake length reduces as the Hartmann number increases. This can be explained by the fact that an imposed magnetic field in the transverse direction of the flow of a conducting fluid induces Lorentz force in the upstream direction. This force has a tendency to suppress the diffusion of vortices out of the wall and, hence, shortens the wake. Figure 3(a-c) shows the temporal variation of the lift coefficient at different Hartmann numbers for Reynolds number of 50. The figure shows that the average lift coefficient is constant at zero after an initial transient period. The time histories of the lift coefficient at different Hartmann numbers confirm that in each case the flow has reached a time-independent steady state and is symmetric about the centerline. However, the time to reach the steady state decreases with increase in the Hartmann number. The time variation of the average drag coefficient at Reynolds number 50 with different Hartmann numbers is shown in Figure 4(a-c). The drag coefficient also confirms the steady nature of the flow. These results show that the steady state is reached quicker as the magnetic field strength increases. In addition, it is observed that the average drag coefficient increases marginally with increase in Hartmann number. It may be attributed to the fact that the increased amount of Lorentz force increases the pressure drop to keep on the flow with fixed discharge. This increase in pressure drop due to significant increase in pressure on the front contributes to the increase in the pressure drag on the body.

The flow at Re = 250 without an imposed magnetic field is time-dependent with a very long wake due to alternate ‘shedding of vortices’ from the lower and upper part of the circular cylinder. The instantaneous streamline pattern for this case is shown in Figure 5(a). The streamline patterns for various imposed transverse magnetic fields are shown in Figure 5(a-d). The snapshots of streamlines show that the flow remains unsteady with periodic vortex shedding up to a certain Hartmann number beyond which the flow become steady with a closed wake and with further increase in Hartmann number the wake length decreases. Since the strength of the shed vortices falls with the gradual increase of the Hartmann number, the flow asymmetry and the amplitude of the lift coefficient decrease as shown in Figure 6(a-b). With further increase of the Hartmann number the vortex shedding process is

eliminated and the flows as presented in Figure 5(c-d) are steady, symmetric and characterized by closed wakes. The cylinder is subjected to zero lift, shown in Figure 6 (c-d), as in very low Reynolds number flow. The evolution of the drag coefficient at different Hartmann numbers presented in Figure 7(a-d) also reflects the change in the flow regime. There is considerable fluctuation in the drag coefficient when no magnetic force is acting but the fluctuation is significantly reduced at H_m = 2.0. The flow remains unsteady at H_m = 2.0 but the amplitude of oscillations of both the lift and drag coefficient has considerably decreased compared to the 'no imposed magnetic field'. This implies that the strength of the shed vortices and the resulting flow asymmetry that essentially generates the lift has decreased. This feature of the flow has also been observed in the streamline plots in Figure 5(a-d). With stronger magnetic field corresponding to H_m = 5.5, the periodic vortex shedding and the consequent unsteadiness and flow asymmetry are eliminated, as evident from the lift and drag coefficient histories in Figures 6(c) and 7(c) respectively. The same physical process that shortens the wake also weakens the shed vortices and finally suppresses the shedding if the Lorentz force is strong enough. It can be concluded that the amplitude of cross flow vibration will reduce significantly for an elastically mounted cylinder with increase in Hartmann number and the vibration can be eliminated if the Hartmann number is increased appropriately. With further increase in the Hartmann number, the length of the attached wake decreases and the drag coefficient slightly increases. The change in the average drag coefficient due to the change in magnetic field strength shows a very striking result. It is observed that the average drag coefficient decreases marginally with increase in the Hartmann number as long as the flow remains unsteady with alternate periodic vortex shedding. This marginal drop in drag force can be attributed to the weakened shed vortices that nullify the effect of increased pressure drop. However, once the flow becomes steady due to sufficiently strong magnetic field the average drag coefficient increases with further increase in Hartmann number due to the increased pressure drop.

The range of minimum Hartmann numbers within which the periodic vortex shedding is completely suppressed and the initial unsteady flow converts to a steady flow at different Reynolds numbers are given in the Table 2. It is seen that the unsteady flow at higher Reynolds numbers need stronger magnetic field to become steady. It is also observed that the threshold or critical Hartmann number for suppressing the shedding of vortices completely is marginally higher for the circular cylinder compared to a square cylinder (Singha et al. 2007). The difference is negligible at the Reynolds number of 150, but increases slowly with increasing Reynolds number. The difference in terms of the actual magnetic strength is still quite small. The most important point, however, is that the shedding can be eliminated in both cases with a relatively weak magnetic field.

The instantaneous vorticity contours at different Hartmann numbers for Reynolds number of 250 are presented in Figure 8(a-g). It is already seen that the flow at $\mathrm{Re} = 250$ remains unsteady for $H_m \le 5.0$ but becomes steady in the range $5 < H_m < 5.5$. The vortex patterns confirm the observation. In the unsteady regime, the alternate periodic vortex shedding from the cylinder is evident. However, the arrangement of the vortices in the wake is opposite to the classic Karman vortex-street wake that forms in an unbounded flow. In the unconfined flow, the vortices of negative and positive sign shed off the upper and lower portion of the cylinder respectively and lie above and below the centerline in a staggered vortex array which is the key structure of the Karman vortex-street. The vorticity contours shown in Figure 8(a-f) reveal that as usual the vortices of negative and positive sign shed from the upper and lower portion of the cylinder respectively. However, the arrangement of the vortices is opposite to

the classic Karman vortex street at a little distance downstream with regard to their vertical positions. It seems that the opposite-signed vortices associated with the shear layer of the near wall repel the shed vortices to switch side. Subsequently, the shed vortices attract the same-signed vortices in the shear layer of the other side. The interacting effect of the cylinder wake vortices on the wall boundary layer growth is evident in the vorticity contours shown in the figure. The nearly periodic acceleration and deceleration induced by the wake vortices affects the growth of the wall shear layer downstream of the cylinder to give it an unsteady undulating appearance. These features are essentially associated with the presence of the solid walls as can be concluded from the vorticity contours in Figure 8(a) corresponding to the 'no magnetic field' case. Zovatto and Pedrizzetti [2001] have reported identical vortex structure in the wake of a circular cylinder confined between two parallel plane walls. These features of the confined flow are maintained in the presence of imposed magnetic field below the critical strength. However, with increasing magnetic field strength the interaction greatly reduces as seen in Figure 8(d-f). Finally, the vortex shedding and flow unsteadiness ceases as the Hartmann number reaches the critical value.

Figure 9(a) shows the variation in the length of the attached wake in the steady flow regime with Hartmann number for several Reynolds numbers. It is observed that at a fixed Reynolds number the wake length decreases significantly with increase in Hartmann number. The variation is nearly linear within the selected ranges of the parameters. In this respect the flow behaviour is identical to the flow about a square cylinder (Singha et al., 2007). The variations in Strouhal number with Hartmann number for different Reynolds numbers are presented in Figure 9(b). The imposed magnetic field does not appreciably affect the frequency of vortex shedding in case of flow over a circular cylinder and the Strouhal number remains almost constant for Hartmann numbers below the critical value. This feature of the circular cylinder flow is in contrast with the square cylinder flow where the Strouhal number increases with Hartmann number until the critical value is reached. The increase is marginal at the lower Reynolds numbers but is considerable at the higher Reynolds numbers (Singha et al., 2007).

Figure 10 presents the dependency of the average drag coefficient on the Hartmann number at different Reynolds number. The drag coefficient increases steadily with increasing Hartmann number in the steady flow regime. The increase is initially slow for Hartmann numbers little over the critical value but at higher Hartmann number the increase in drag coefficient is quite rapid. In the unsteady regime, the drag coefficient decreases marginally with increasing magnetic field strength.

Conclusions

Low Reynolds number laminar flows around a confined circular cylinder subjected to an imposed uniform transverse magnetic field are studied using an unstructured collocated grid finite volume implicit incompressible Navier-Stokes solver. The fluid is assumed to have a uniform electrical conductivity. The induced magnetic field is assumed to be negligible in comparison with the imposed magnetic field which is justified for MHD flows at very small magnetic Reynolds numbers. It is observed that in the closed attached wake regime of the flow the wake length decreases approximately linearly with increase in Hartmann number. In the periodic wake regime the vortex shedding and unsteadiness reduces as the Hartmann number increases and if a sufficiently strong magnetic field is applied the vortex shedding is suppressed. The limiting Hartmann number at which shedding is suppressed increases with

Reynolds number. The limiting Hartmann number is marginally greater for circular cylinder flows compared to square cylinder flows. The difference increases with Reynolds number. The interaction between the vortices shed from the cylinder and wall shear layer is also found to decrease with increasing Hartmann number. With increasing Hartmann number the drag coefficient is found to decrease marginally in the unsteady flow regime but to increase considerably in the steady flow regime. At a Reynolds number of 150 the mean drag coefficient falls by nearly 4% as the Hartmann number increases from 0.0 to 2.5 and subsequently increases by 48% at Hartmann number of 6.5. The drag coefficient increases more rapidly at higher Hartmann numbers. The amplitude of the periodic lift coefficient decreases with increase in Hartman number and falls to zero at the limiting Hartmann number. It is seen that the Strouhal number at a fixed Reynolds number is insensitive to the change in Hartmann number as long as the flow remains unsteady. This characteristic of the flow about circular cylinder is in contrast to the flow about square cylinder.

References

1. Bramley JS. Magnetohydrodynamic flow past a circular cylinder. *Journal of Applied Mathematics and Physics ZAMP* 1974; 25 (3), 409-416.
2. Bramley JS. Magnetohydrodynamic flow past a circular cylinder II. *Journal of Applied Mathematics and Physics ZAMP* 1974; 26 (2), 203-209.
3. Gerbeth G, Thess A, Marty P. Theoretical study of the MHD flow around a cylinder in crossed electric and magnetic fields, *Europ. Journ. of Mech.,* 9, #3, p.239-257, 1990.
4. Josserand J, Marty Ph, Alemany A. Pressure and drag measurements on a cylinder in a liquid metal flow with an aligned magnetic field. *Fluid Dynamic Research* 1993; 11, 107–117.
5. Mutschke G, Shatrov V, Gerbeth G. Cylinder wake control by magnetic fields in liquid metal flows. *Experimental Thermal and Fluid Science* 1998; 16, 92-99.
6. Midya C, Layek GC, Gupta AS, Mahapatra RT. Magnetohydrodynamic viscous flow separation in a channel with constriction. *ASME Journal of Fluids Engineering* 2003, 125, 952-962.
7. Sekhar TVS, Sivakumar R, Ravikumar TVR. Flow around a circular cylinder in an external magnetic field at high Reynolds numbers, *International Journal of Numerical Methods for Heat & Fluid Flow,* 16, 740-759, 2006.
8. Singha S, Sinhamahapatra KP, Mukherjea SK. Control of vortex shedding from a bluff body using imposed magnetic field. *ASME Journal of Fluids Engineering* 2007; 129, 517-523.
9. Knaepen B, Kassinos SC, Carati D. MHD turbulence at moderate magnetic Reynolds number. *Journal of Fluid Mech.*, 513, 199-220, 2004.
10. Kassinos SC, Carati D, Knaepen B. The transport of a passive scalar in MHD turbulence subjected to mean shear and frame rotation. *Physics of Fluids*, 19, 015105-(1-23), 2007, DOI: 10.1063/1.2409732
11. Saaris I, Kassinos SC, Carati D. Large-Eddy Simulations of the turbulent Hartmann flow close to the transitional regime. *Physics of Fluids*, 19, 085109-(1-9), 2007, DOI: 10.1063/1.2757710.
12. Zovatto L, Pedrizzetti G. Flow about a circular cylinder between parallel walls. *Journal of Fluid Mechanics* 2001; 440, 1-25.

13. Shercliff JA. *A Textbook of Magnetohydrodynamics*. Pergamon Press, New York, 1965.
14. Rhie CM, Chow WL. A numerical study of the turbulent flow past an isolated airfoil with trailing edge separation. *AIAA Journal* 1983; 21, 1525 –1532.
15. Leonard BP. A stable and accurate convective modeling procedure based on quadratic upstream interpolation. *Computational Methods in Applied Mechanics and Engineering* 1979; 19, 59-98.
16. Holmes DG, Connel SD. Solution of 2D Navier-Stokes equations on unstructured adaptive grids. *AIAA paper 89-1932-CP* 1989.
17. Zhou CY, So RMC, Lam K. Vortex-induced vibration of an elastic circular cylinder. *Journal of Fluids and Structures* 1999; 13**,** 165-189.

Control of Vortex Shedding from a Circular Cylinder using Imposed Transverse Magnetic Field

Sintu Singha
Department of Aerospace Engineering, IIT Kharagpur
Kharagpur 721302, India

singha.sintu@gmail.com

and

K. P. Sinhamahapatra
Department of Aerospace Engineering, IIT Kharagpur
Kharagpur 721302, India

kalyanps@iitkgp.ac.in